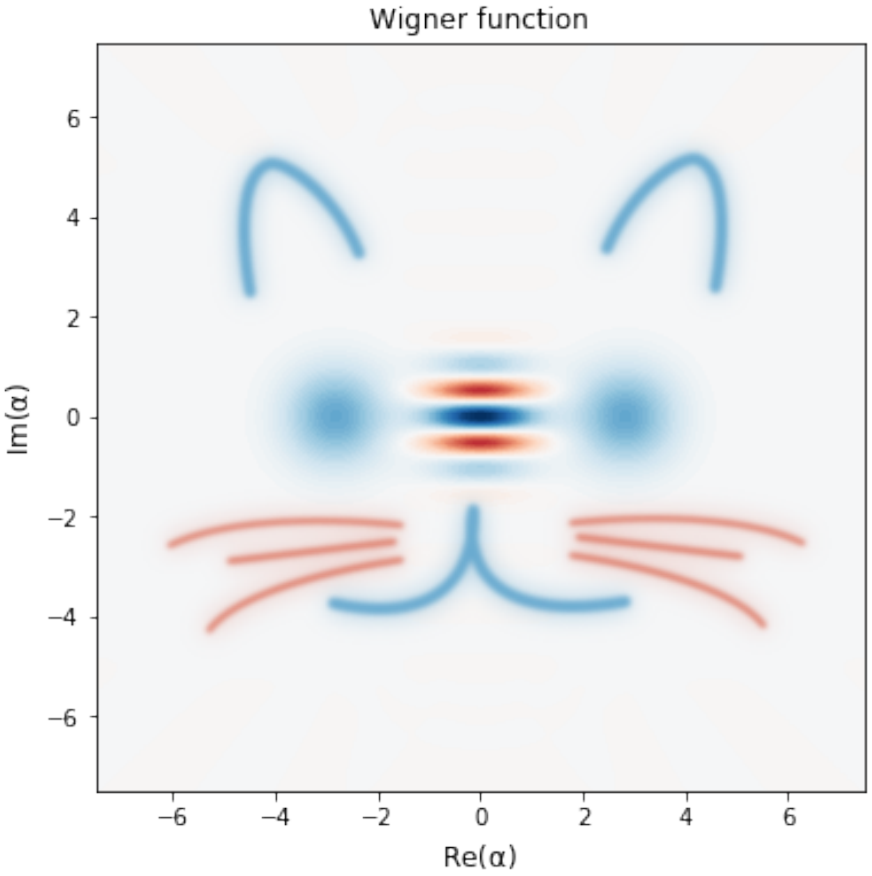

Encoding Qubit States in the Cat Code

A Proof of Concept for Numerically Optimizing Encoding Pulses Using Krotov's Method

Master's thesis in Quantum Computing

JOHAN WINTHER

Department of Microtechnology and Nanoscience
CHALMERS UNIVERSITY OF TECHNOLOGY
Göteborg, Sweden 2019

MASTER'S THESIS IN QUANTUM COMPUTING

Encoding Qubit States in the Cat Code

A Proof of Concept for Numerically Optimizing Encoding Pulses Using Krotov's Method

JOHAN WINTHER

Department of Microtechnology and Nanoscience
Division of Applied Quantum Physics Laboratory
CHALMERS UNIVERSITY OF TECHNOLOGY

Göteborg, Sweden 2019

Encoding Qubit States in the Cat Code
A Proof of Concept for Numerically Optimizing Encoding Pulses Using Krotov's Method
JOHAN WINTHER

Master's thesis 2019:XX
ISSN 1652-8557
Department of Microtechnology and Nanoscience
Division of Applied Quantum Physics Laboratory
Chalmers University of Technology
SE-412 96 Göteborg
Sweden
Telephone: +46 (0)31-772 1000

Cover:
Wigner function of a cat state.

Chalmers Reproservice
Göteborg, Sweden 2019

Encoding Qubit States in the Cat Code
A Proof of Concept for Numerically Optimizing Encoding Pulses Using Krotov's Method
JOHAN WINTHER
Department of Microtechnology and Nanoscience
Division of Applied Quantum Physics Laboratory
Chalmers University of Technology

Abstract

Quantum computing has gained a lot of interest in recent years and commercial products are just now entering the market. However one of the main challenges in realising a quantum computer is noise and one key technology to remedy this is quantum error correction (QEC). One way of performing QEC is to store the quantum information of a qubit, while it's idle, as special basis states in a resonator. To do this one needs to apply encoding and decoding pulses to the coupled qubit-resonator system to do a state transfer. These pulses are hard or perhaps impossible to solve for analytically, which means they need to be numerically obtained by simulation.

This thesis studies the prospects of using Krotov's method (gradient ascent) to numerically optimize encoding pulses for state transfer. The Python package Krotov, a package for quantum optimal control using Krotov's method, is used to perform state transfers $|0\rangle$ to $|1\rangle$ and $|0\rangle$ to $|2\rangle$ of an anharmonic resonator. It is shown that, assuming a maximum drive amplitude and no dissipation, the method can realise a $|0\rangle$ to $|1\rangle$ transfer with fidelity $F > 0.99999$ with a total pulse length of only 10.75 ns. For the $|0\rangle$ to $|2\rangle$ transfer a total pulse length of 30 ns is needed to reach the same fidelity. Thus it is concluded that state transfers using Krotov for non-coupled systems is viable.

However for coupled systems there is great difficulty in using Krotov, as the package assumes a time-independent control Hamiltonian. A potential workaround for this problem is also presented.

Keywords: quantum computing, quantum optimal control, cat state, cat code

Preface

Acknowledgements

I would like to thank cats

Contents

1 Introduction

Quantum computing is starting to appear in commercial products [1], however, despite progress [2], there are still a lot of challenges to be solved before large scale quantum computers become commonplace. Unlike classical computers, where the transistors' on and off state is dictated by the stream of many electrons, quantum computers rely on single or very few number of particles which make the quantum states very delicate [3]. One of the key technologies to keep these states stable is quantum error correction (QEC) [3], which is a way to protect quantum information from noise. One way to do this is to introduce redundancy into the physical system and spread the information to highly entangled states using *quantum error correcting codes*.

Leghtas, Kirchmair, Vlastakis, *et al.* [4], Mirrahimi, Leghtas, Albert, *et al.* [5] propose and Ofek, Petrenko, Heeres, *et al.* [6] demonstrate a method to encode the quantum information in a "cat code" in quantum harmonic resonators. The theory of the cat code presented in section 2.3. To further clarify the encoding scheme, the quantum information of a superconducting qubit is carefully encoded into a cavity resonator by simultaneously driving the qubit and resonator system with microwave pulses. This realises the desired state transfers in both the qubit and the resonator. Ofek, Petrenko, Heeres, *et al.* numerically optimize the microwave pulse shapes using the GRAPE algorithm [7] which uses gradient ascent while simulating the system to update the pulse shapes until the state transfer is realised.

There is no source code available for this method which provides an opportunity to reproduce this result with an easy-to-use open source software package and hopefully provide reference for future implementations.

1.1 Purpose of the Thesis

The purpose of this thesis is to, in simulation, numerically optimize microwave pulses to encode the quantum information of a qubit to the cat code as a proof of concept. The pulses will be optimized using Krotov's method [8], a gradient-based optimization algorithm available publicly as a ready-to-use Python package [9].

The scope of the thesis is limited to

- closed quantum systems without any interaction with the environment,
- assessing the performance of the method without fully understanding the underlying explanations for the results and
- only finding *encoding*-pulses (decoding-pulses introduce additional complexity).

2 Theory

In this chapter theoretical concepts in quantum optics and quantum optimal control will be introduced. First of, the quantum systems used in this thesis will be presented, then the cat code will be presented. After that some important visualization tools for quantum mechanics are shown. Finally, the basics of quantum optimal control are presented. Note however that it is assumed that the reader has at least a basic understanding of quantum mechanics.

2.1 Superconducting resonators

Superconducting resonators are used in quantum computing both as the basis for qubits and as readout and control components. Although ideal resonators have equally spaced energy levels, in reality they are more or less anharmonic and the general Hamiltonian for a quantum anharmonic resonator is

$$\hat{H} = \omega_q \hat{a}^\dagger \hat{a} + \frac{\kappa_q}{2}(\hat{a}^\dagger)^2 \hat{a}^2 \tag{2.1}$$

where ω_q is the resonance frequency, κ_q is the anharmonic (self-Kerr) term and $\hat{a}$ is the destruction operator which removes an excitation from the resonator. Note that this is still an approximation as higher order terms have been neglected.

The anharmonicity can be vizualised, see fig. 2.1, by plotting the eigenenergies of eq. (2.1) as a function of κ. A larger anharmonicity makes the energy spacing larger for excitation states higher than $|1\rangle$. This anharmonicity is what permits a resonator to act as a qubit, as it is possible to adress only the first two states $|0\rangle$ and $|1\rangle$ due to the frequency difference. Throughout this thesis, the term "qubit" will be used to refer to an anharmonic resonator even though it has more than two energy levels. Further, the "resonance frequency of the qubit" which correspond to the energy spacing between the first two levels, will be referred to as ω_q.

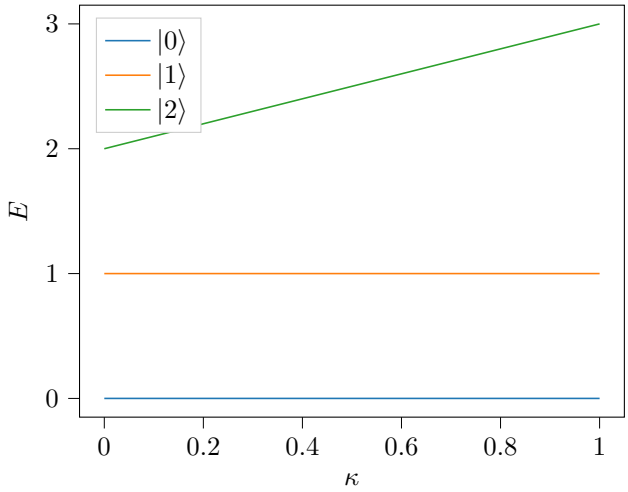

Figure 2.1: The energy levels of a three-level resonator for anharmonicity $\kappa \in [0, 1]$ and $\omega_q = 1$.

2.2 Coupled Qubit-Resonator System

The Hamiltonian for a coupled qubit and resonator is chosen as

$$\hat{H}(t) = \underbrace{\omega_r \hat{a}^\dagger \hat{a} + \frac{\kappa_r}{2}(\hat{a}^\dagger)^2 \hat{a}^2}_{\text{Resonator}} + \underbrace{\omega_q \hat{b}^\dagger \hat{b} + \frac{\kappa_q}{2}(\hat{b}^\dagger)^2 \hat{b}^2}_{\text{Qubit}} + \underbrace{g\left(\hat{a}^\dagger \hat{b} + \hat{a}\hat{b}^\dagger\right)}_{\text{Coupling}} \tag{2.2}$$

where $\hat{b}$ is the destruction operator for the qubit. There is now a coupling term with the coupling strength g which means that the resonator and the qubit can exchange excitations between each other. g will be assumed

to be real for simplicity. This is similar to the Jaynes-Cummings Hamiltonian, but now there are added self-Kerr terms for both the qubit and the resonator. Another difference is that the Jaynes-Cummings model explicitly deals with a two-level qubit or atom, while this model has a "qubit" with arbitrary levels. Note that the rotating wave approximation has been applied to the coupling term [10].

2.3 Cat code

The cat code is a logical basis for quantum information stored in resonators. The basis states are

$$|0_L\rangle = |C_{\ \alpha}\rangle\,, \quad |1_L\rangle = |C_{i\alpha}\rangle \tag{2.3}$$

where

$$\left|C_{(i)\alpha}\right\rangle = \frac{1}{\sqrt{2}}(|(i)\alpha\rangle + |-(i)\alpha\rangle). \tag{2.4}$$

That is the each basis state $|0(1)_L\rangle$ in the cat code consists of a cat state $\left|C_{(i)\alpha}\right\rangle$, which is a superposition of a coherent state $|(i)\alpha\rangle$ and its negative counterpart $|-(i)\alpha\rangle$. A coherent state can be represented in the Fock basis as

$$|(i)\alpha\rangle = \mathrm{e}^{-\frac{|(i)\alpha|^2}{2}} \sum_{n=0}^{\infty} \frac{((i)\alpha)^n}{\sqrt{n!}} |n\rangle\,. \tag{2.5}$$

The basis can also be in an odd parity where the two coherent states are subtracted instead of added, however only the even parity basis will be used in this thesis. A more detailed review of the cat code can be found in the supplementary information of [6].

2.4 Visualization of quantum states

In order to understand the results presented later in this thesis, some visualization techniques of quantum states are shown and explained.

2.4.1 Bloch sphere

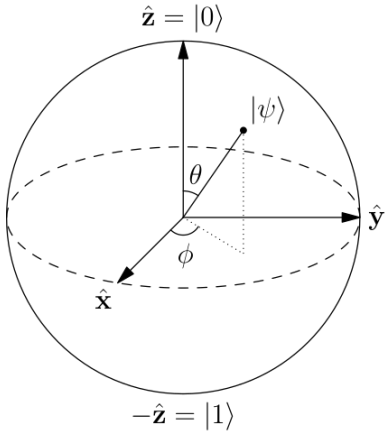

Figure 2.2: Representation of an abritrary pure quantum state on the Bloch sphere.
Source: [11] (CC BY-SA 3.0).

The pure state of a qubit can be visualized on the surface of a unit sphere with the following parametrization

$$|\psi\rangle = \cos\left(\frac{\theta}{2}\right)|0\rangle + \mathrm{e}^{i\phi}\sin\left(\frac{\theta}{2}\right)|1\rangle \tag{2.6}$$

where θ and ϕ are angles which are shown in fig. 2.2. The ground state $|0\rangle$ is located on the "north pole" and the excited state $|1\rangle$ on the "south pole".

Further, a handy trick to visualize the qubit when it has more levels than three is to "project" the state to the $\{|0\rangle, |1\rangle\}$ basis with $|0\rangle\langle 0| + |1\rangle\langle 1|$ and then plot it on the Bloch sphere. This means that the subspace which is not spanned by the first two levels will be represented by the inside of the sphere. To make an example, $|2\rangle$ will lie right in the center of the sphere while $(|1\rangle + |2\rangle)/\sqrt{2}$ will lie halfway between the center and the south pole.

2.4.2 Wigner function

The wigner function can be used to visualize quantum states and processes. It is a quasiprobability distribution where states exhibiting quantum phenomena will have negative values, impossible for classical states.

To give a visual example, 6 example states in the cat code basis are shown in fig. 2.3 with $\alpha = 2$ and a Hilbert space size of $N_r = 8$. Looking at $|0\rangle$ we can see two lobes with an interference fringe in between them. For large enough N_r there will be no truncation of the Hilbert space and the lobes will appear circular. Compared to the basis states, the superposition states exhibit even more complex shapes.

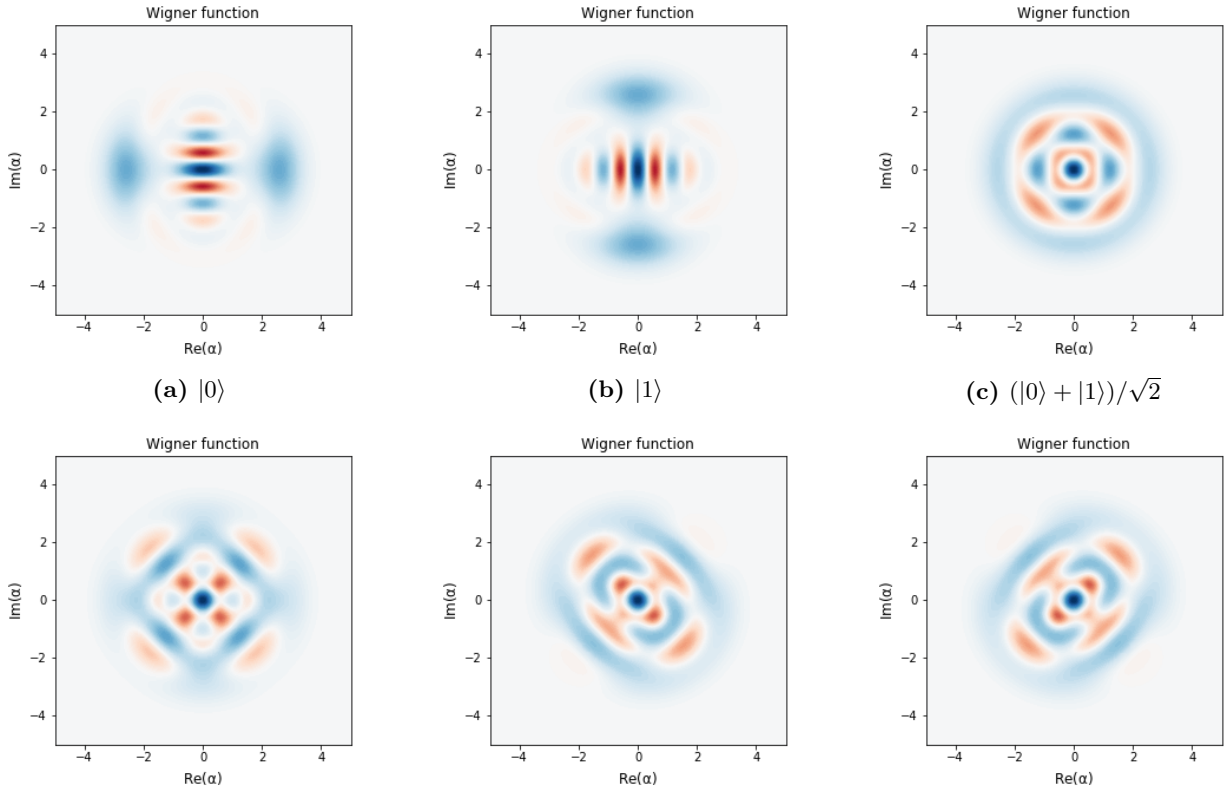

(a) $|0\rangle$ **(b)** $|1\rangle$ **(c)** $(|0\rangle + |1\rangle)/\sqrt{2}$

(d) $(|0\rangle - |1\rangle)/\sqrt{2}$ **(e)** $(|0\rangle + i\,|1\rangle)/\sqrt{2}$ **(f)** $(|0\rangle - i\,|1\rangle)/\sqrt{2}$

Figure 2.3: Wigner function of some example states in the cat code basis with $\alpha = 2$ and $N_r = 8$.

2.5 Quantum optimal control

Quantum control is the process of controlling a quantum system by controlling the amplitude of a set of control operators [12]. Such a system can be described [12] by a Hamiltonian of the following form

$$\hat{H}(t) = \underbrace{\hat{H}_d}_{\text{Drift}} + \underbrace{u_0(t)\hat{H}_0 + \ldots + u_N(t)\hat{H}_N}_{\text{Control}}. \tag{2.7}$$

The controls are usually electromagnetic pulses changing in time and thus will be referred to as "pulse shapes" [12] in this thesis .

There are two main questions in quantum control: one of *controllability* and one of *optimal control*. The first deals with the *existence* of solutions given a Hamiltonian and the second with the *optimized* solutions for the pulse shapes $\{u_i(t)\}$ [13]. The optimal solutions are generally not analytically solvable and thus the pulse shapes need to be discretized in time and numerically optimized using algorithms. The algorithm used for this thesis is called Krotov's method and will be presented in the Method chapter.

2.5.1 Unitary transformation

A unitary transformation can drastically simplify systems that are hard to simulate. This idea will be conceptually presented here and then implemented in the Method chapter. The transformation that is used is a special case of unitary transformations called the *interaction picture* where the Hamiltonian is split up into a time-independent and time-dependent part

$$\hat{H}(t) = \hat{H}_A + \hat{H}_B(t). \tag{2.8}$$

By choosing the unitary operator $\hat{U} = \mathrm{e}^{i\hat{H}_A t}$ the unitary transformation takes us into the interaction picture

$$\begin{aligned}
\hat{H} \rightarrow\ & \hat{U}\Big[\hat{H}_A + \hat{H}_B(t)\Big]\hat{U}^\dagger + i\frac{\mathrm{d}\hat{U}}{\mathrm{d}t}\hat{U}^\dagger = \\
=\ & \hat{U}\hat{H}_A\hat{U}^\dagger + \hat{U}\hat{H}_B\hat{U}^\dagger + i\Big(i\hat{H}_A t\Big)\mathrm{e}^{i\hat{H}_A t}\mathrm{e}^{-i\hat{H}_A t} = \\
=\ & \hat{H}_A + \hat{U}\hat{H}_B\hat{U}^\dagger - \hat{H}_A = \hat{U}\hat{H}_B\hat{U}^\dagger
\end{aligned}$$

3 Method

In this chapter Krotov's method for quantum optimal control will be briefly introduced and an implementation as a Python package. Then the numerical experiments will be explained.

3.1 Krotov's Method for Quantum Optimal Control

Krotov's method for quantum control fundamentally relies on the variational principle to minimize a functional

$$J\left[\left\{\left|\phi_k^{(i)}(t)\right\rangle\right\}, \left\{u_l^{(i)}(t)\right\}\right]$$

that depends on the pulse shapes and the quantum states of the system evolved under these pulse shapes [9]. A detailed explanation of this functional can be found in [8]. However a quick summary of how the method works will be presented here. Starting with some guess pulse shapes, the initial state is forward propagated in time using a Hamiltonian of the same form as eq. (2.7) and the value of the functional is calculated. Then changes to the pulse shapes which will decrease the value of the functional are calculated, by propagating states with these new pulse shapes, and these updates become the new pulse shapes. This continues until convergence is reached.

The underlying mathematical principles of Krotov's method will not be adressed in the thesis, as that is outside the scope. Therefore the method will be treated as a black box function provided by the Python package which will be presented in the next section.

3.1.1 Krotov: the Python package

A Python implementation of the Krotov's method is available at [9] which provides an abstraction layer for doing optimizations. The package will be referred to as `krotov`. The reason `krotov` was chosen is primarily because it allows for optimization of multiple objectives simultaneously. This is necessary in order to create a single encoding pulse which will realise the state transfer into the cat code basis for any arbitrary state.

The package is built on top of QuTiP, a popular software package for simulating the dynamics of quantum systems [14]. That means it can leverage all the useful features of that package, which is also another reason this method was chosen. The package provides a set of submodules which are used to setup the optimization problem. The important modules will be presented here.

The `objectives` module describes the goal of the optimization, be it a state-to-state transfer or a quantum gate. It is used to specify the initial and target states, the Hamiltonian and the initial guess pulses.

The `functionals` module provides a set of functionals which can be used for Krotov's method. In this work the functional `chis_ss` has been chosen for all optimizations.

In the `convergence` module, help functions for the stopping criteria are provided for the optimization. It exposes values such as the overlap of the forward propagated state and target state $\langle\psi(T)|\psi^{\text{tar}}\rangle$ during the optimization which can be used to check when convergence is reached. The stopping criteria chosen for this thesis is either a minimum fidelity

$$F = \frac{1}{S}\sum_{k=1}^{S} |\left\langle\psi_k(T)\middle|\psi_k^{\text{tar}}\right\rangle|^2, \tag{3.1}$$

where S is the number of (simultaneous) state transfers we want to realise, or when the change in fidelity between iterations ΔF falls below a specified value (where a local minimum can be assumed to have been reached). The values of these will be specified in section 3.2

Finally, the `optimization` module is used to setup the whole optimization. It is possible to choose the time discretization, convergence criteria, optimization functional, and a function which will run after every iteration. Also the step size $1/\lambda$ of the pulse updates can be chosen which is further explained in [9]. Note however that although a large step size could achieve faster convergence, it can also lead to numerical instability.

3.2 Optimization Experiments

In this chapter the numerical optimization experiments are presented and motivated. The first experiment was used to assess the viability of the method, while the last one is a proof of concept for encoding states into

the cat code basis. All optimizations were run on a Lenovo Yoga 520-14IKB PC with an Intel(R) Core(TM) i7-8550 CPU running Windows 10.

3.2.1 Qubit state transfers

In this experiment, the optimization was run to realise the state transfer $|0\rangle \to |1\rangle$ and then $|0\rangle \to |2\rangle$. The first transfer should be close to the ideal solution of a π-pulse, while the second is non-trivial. Therefore they are suitable goals to test the method and package.

Hamiltonian

The anharmonic resonator (qubit) in eq. (2.1) was chosen as it is a simple model for a physical qubit. As stated earlier such a system will be referred to as a qubit even though it has more than two energy levels. To induce transitions between the states of the qubit, control pulse terms were added to eq. (2.1)

$$\hat{H} = \omega_q \hat{a}^\dagger \hat{a} + \frac{\kappa_q}{2}(\hat{a}^\dagger)^2 \hat{a}^2 + \Omega(t) \mathrm{e}^{-i\omega_q t} \hat{a} + \Omega^*(t) \mathrm{e}^{i\omega_q t} \hat{a}^\dagger \tag{3.2}$$

where $\Omega(t)$ is the complex amplitude of the control pulse. Looking at the Hamiltonian above it can be argued that it can be written in the form in eq. (2.7), which is needed by `krotov`, with $u_0(t) = \Omega(t)\mathrm{e}^{i\omega_q t}$ and $u_1(t) = \Omega^*(t)\mathrm{e}^{-i\omega_q t}$. However, there are two problems that need to be adressed. Firstly, the oscillating factors require an unnecessarily fine time discretization of the pulses. Secondly, the Krotov package expects real-valued pulse amplitudes $\{u_i(t)\}$ as inputs. The first problem was avoided by transforming the Hamiltonian into the interaction picture. Choosing $H_A = \omega_q \hat{a}^\dagger \hat{a}$, eq. (3.2) transforms[1] into

$$\hat{H} \to \frac{\kappa_q}{2}(\hat{a}^\dagger)^2 \hat{a}^2 + \Omega(t)\hat{a} + \Omega^*(t)\hat{a}^\dagger. \tag{3.3}$$

Now the pulse amplitudes were $u_0(t) = \Omega(t)$ and $u_1(t) = \Omega^*(t)$, i.e. the envelope of the physical control pulse which varies significantly slower than the actual pulse. The second problem was easily fixed with a rearrangment of the terms

$$\Omega(t)\hat{a} + \Omega^*(t)\hat{a}^\dagger = \Big[\mathrm{Re}[\Omega(t)] + i\mathrm{Im}[\Omega(t)]\Big]\hat{a} + \Big[\mathrm{Re}[\Omega(t)] - i\mathrm{Im}[\Omega(t)]\Big]\hat{a}^\dagger =$$

$$= \mathrm{Re}[\Omega(t)]\big(\hat{a} + \hat{a}^\dagger\big) + \mathrm{Im}[\Omega(t)] i\big(\hat{a} - \hat{a}^\dagger\big).$$

For intuition, $\big(\hat{a} + \hat{a}^\dagger\big)$ and $i\big(\hat{a} - \hat{a}^\dagger\big)$ correspond to Bloch sphere rotations around the x-axis and y-axis respectively. Thus the final Hamiltonian became

$$\hat{H} = \underbrace{\kappa_q/2(\hat{a}^\dagger)^2\hat{a}^2}_{\hat{H}_d} + \underbrace{\mathrm{Re}[\Omega(t)]}_{u_0(t)}\underbrace{(\hat{a} + \hat{a}^\dagger)}_{\hat{H}_0} + \underbrace{\mathrm{Im}[\Omega(t)]}_{u_1(t)}\underbrace{i(\hat{a} - \hat{a}^\dagger)}_{\hat{H}_1}. \tag{3.4}$$

The parameters of the qubit were chosen to model real superconducting qubits with $\kappa_q = 2\pi \times 297\,\mathrm{MHz}$ (and $\omega_q = 2\pi \times 6.2815\,\mathrm{GHz}$). The system Hamiltonian in eq. (3.4) was simulated with a Hilbert space size conveniently chosen to be $N_q = 3$. A smaller Hilbert space, and consequently smaller matrices, requires less computations but could possibly be a poor approximation of the Hamiltonian. Thus the solutions of the optimization were analysed with this in mind.

Optimization Setup

As the long-term goal is to use this method in physical systems some constraints were added. To simulate the constraints of physical **a**rbitrary **w**aveform **g**enerators a maximum sample rate of $4\,\mathrm{GSa\,s^{-1}}$ was chosen. Recall that the physcal pulses oscillate at $\omega_q = 6.2815\,\mathrm{GHz}$, a rate which $4\,\mathrm{GSa\,s^{-1}}$ can impossibly resolve. Although AWGs with higher sample rates than $4\,\mathrm{GSa\,s^{-1}}$ exist, they are expensive. However, rotating frame transformation permits the use of a relatively low rate AWG to generate the pulse envelopes $\Omega(t)$ and a high rate tone generator to create a carrier signal at ω_q, with these signals later combined in a mixer. Further, due to the noise sensitivity of superconducting systems an amplitude constraint is needed to keep the system

[1] Full derivation is shown in **??**

cool enough. To set a realistic maximum amplitude A_m some derivation was required. First the maximum amplitude was chosen with the assumption that a gaussian pulse

$$g(t) = \frac{\pi/2}{\sigma\sqrt{2\pi}} \mathrm{e}^{-\frac{1}{2}\left(\frac{t}{\sigma}\right)^2} \tag{3.5}$$

with $\sigma = 3\,\mathrm{ns}$ can physically realise a π-rotation $|0\rangle \to |1\rangle$ in a planar transmon qubit. The problem with gaussian pulses however is that they don't go to zero at the edges. To fix this `krotov` provides a function for generating Blackman pulses. A Blackman pulse with a total length of 6σ is a good approximation of a Gaussian pulse, with the added benefit of going to zero at the edges. However, due to the approximation, the integral of the Blackman pulse will not exactly be equal to the integral of the corresponding gaussian pulse, which is needed to realise the π-rotation. This can be fixed by using a prefactor C which can be calculated by solving

$$C \int_0^{6\sigma} \frac{1}{\sqrt{2\pi}\sigma} B(t) = \int_0^{6\sigma} g(t - 3\sigma)\,\mathrm{d}t \tag{3.6}$$

where $B(t)$ is the Blackman pulse. This is now used to determine the maximum amplitude

$$A(\sigma) = \frac{C}{\max(\sigma, 3)\sqrt{2\pi}} \tag{3.7}$$

with $A_m = A(\sigma = 3)$. This axmplitude constraint is enforced by calling a function after every iteration which limits all pulse shape values $|\Omega| < A_m$. Conveniently, the Blackman pulse was also used as the initial guess pulse with $u_0(t) = A(T/6)B(t)$.

Another constraint is that the edges of the pulses should always be zero with a switch-on/switch-off of 2 ns. This ramp shape is half a Blackman pulse and is provided by `krotov`'s `flattop` function.

For the $|0\rangle \to |1\rangle$ state transfer pulse shapes were optimized with varying lengths from 4.25 ns to 30 ns with convergence criteria $F > 0.99999$ or $\Delta F < 10^{-7}$. The step size was chosen as $\lambda = \frac{1}{\frac{1}{2}A_m}$. The reason for optimizing for various pulse lengths was that faster pulse changes gives a broader support in the frequency spectrum which can ultimately induce transitions in other levels. Therefore the optimization needs to find a solution which circumvents this problem.

Lastly, for the $|0\rangle \to |2\rangle$ state transfer pulse shapes were optimized with varying lengths from 22 ns to 30 ns with convergence criteria $F > 0.99999$ or $\Delta F < 10^{-9}$. The low ΔF was needed because the changes were very small in the beginning of the optimization. The step size was chosen as $\lambda = \frac{1}{2A_m}$ due to slow convergence. In contrast to the $|0\rangle \to |1\rangle$ state transfer both initial guess pulses were chosen to be Blackman pulses $u_0(t) = u_1(t) = A(T/6)B(T)$.

3.2.2 Cat code encoding

For the cat code encoding, 6 simultaneous objectives were chosen to give encoding pulses which maps the 6 furthest states on the Bloch sphere to the corresponding resonator states. These initial qubit states are (omitting normalization)

$$|0\rangle, |1\rangle,$$

$$|0\rangle + |1\rangle, |0\rangle - |1\rangle,$$

$$|0\rangle + i\,|1\rangle, |0\rangle - i\,|1\rangle$$

with target state $|0\rangle$, and the resonator initial state is $|0\rangle$ with target states

$$|C_{\ \alpha}\rangle, |C_{i\alpha}\rangle,$$

$$|C_{\ \alpha}\rangle + |C_{i\alpha}\rangle, |C_{\ \alpha}\rangle - |C_{i\alpha}\rangle,$$

$$|C_{\ \alpha}\rangle + i\,|C_{i\alpha}\rangle, |C_{\ \alpha}\rangle - i\,|C_{i\alpha}\rangle.$$

In summary the pulse shapes will realise the unitary

$$\hat{U}(T)(c_0\,|0\rangle + c_1\,|0\rangle) \otimes |0\rangle = |0\rangle \otimes (c_0\,|C_{\ \alpha}\rangle + c_1\,|C_{i\alpha}\rangle). \tag{3.8}$$

Hamiltonian

In this experiment the coupled qubit-resonator system in eq. (2.2) was used. As the operators $\hat{a}$ and $\hat{b}$ commute, eq. (3.4) was also used for the extra resonator. The rotating frame transformation is done with respect to $H_A = \omega_r \hat{a}^\dagger \hat{a} + \omega_q \hat{b}^\dagger \hat{b}$. However as the coupling term has no time dependence and does not commute with the operators there will still be a time dependence in the rotating frame

$$g(\hat{a}\hat{b}^\dagger + \hat{a}^\dagger \hat{b}) \to g(\hat{a}\hat{b}^\dagger \mathrm{e}^{i(\omega_q - \omega_r)t} + \hat{a}^\dagger \hat{b} \mathrm{e}^{-i(\omega_q - \omega_r)t}). \tag{3.9}$$

This was a problem because `krotov` expects $\hat{H}_d$ to be time independent. There is a way to "simulate" the coupling term by inserting it as an external time dependent pulse and omit it from optimization which was done in this case. The coupling term was then split into a real and imaginary part which is, as stated before, required by `krotov`.

The final Hamiltonian provided to `krotov` was then

$$\begin{aligned}
\hat{H} = & \underbrace{\kappa_r/2(\hat{a}^\dagger)^2\hat{a}^2 + \kappa_q/2\left(\hat{b}^\dagger\hat{b}\right)^2}_{\hat{H}_d} + \\
& + \underbrace{\mathrm{Re}[\Omega_r(t)]}_{u_0(t)} \underbrace{(\hat{a} + \hat{a}^\dagger)}_{\hat{H}_0} + \underbrace{\mathrm{Im}[\Omega_r(t)]}_{u_1(t)} \underbrace{i(\hat{a} - \hat{a}^\dagger)}_{\hat{H}_1} + \underbrace{\mathrm{Re}[\Omega_q(t)]}_{u_2(t)} \underbrace{(\hat{b} + \hat{b}^\dagger)}_{\hat{H}_2} + \underbrace{\mathrm{Im}[\Omega_q(t)]}_{u_3(t)} \underbrace{i(\hat{b} - \hat{b}^\dagger)}_{\hat{H}_3} + \\
& + \underbrace{[\cos((\omega_q - \omega_r)t)]}_{u_4(t)} \underbrace{g(\hat{a}\hat{b}^\dagger + \hat{a}^\dagger\hat{b})}_{\hat{H}_4} + \underbrace{[\sin((\omega_q - \omega_r)t)]}_{u_5(t)} \underbrace{ig(\hat{a}\hat{b}^\dagger - \hat{a}^\dagger\hat{b})}_{\hat{H}_5}
\end{aligned} \tag{3.10}$$

The parameters of this system is presented in table 3.1.

Table 3.1: Hamiltonian parameters

Param.	Value
$\omega_q/(2\pi)$	6.2815 GHz
$\kappa_q/(2\pi)$	297 MHz
$\omega_r/(2\pi)$	8.3056 GHz
$\kappa_r/(2\pi)$	4.5 kHz
$g/(2\pi)$	1.413 GHz

The Hilbert space size for the resonator was chosen to be $N_r = 8$ with the mean photon number $\alpha = 2$. Due to the large system size, the qubit Hilbert space size was set to $N_q = 2$.

Optimization setup

The optimization was setup in the same way as the previous experiment, however due to the rapid oscillations at $|\omega_q - \omega_r|$ a finer time discretization of $24\,\mathrm{GSa\,s^{-1}}$ was chosen. The step size was chosen as $\lambda = \frac{1}{\frac{1}{2}A_m}$ and the pulse length $T = 60\,\mathrm{ns}$ to allow the coupling to affect the system. Further, convergence criteria was chosen as $F > 0.999999$ or $\Delta F < 10^{-6}$. Another important step in optimizing in the rotating frame was to convert the target states into the rotating frame by multiplying with $U^\dagger = \mathrm{e}^{i\hat{H}_A T}$. This was needed for the final states to be correct in the lab frame. Initial guess pulses were chosen to be a Blackman pulse corresponding to a π-rotation of the qubit in the previous experiment.

4 Results

The results of the numerical experiments will be presented in this chapter. For both optimization targets the optimized pulses, their properties and the final evolved state will be presented.

4.1 Qubit state transfers

4.1.1 $|0\rangle \rightarrow |1\rangle$ state transfer

In fig. 4.1 the fidelity during all optimization runs are plotted. For pulse lengths longer than 15 ns the fidelity starts at values close to the goal ($F > 0.9$) and the number of iterations is relatively low (less than 85 iterations). In contrast, pulses shorter than 15 ns start at lower fidelities while the number of iterations are roughly one order of magnitude larger with no clear pattern with respect to the pulse length.

To give a more detailed picture, the starting fidelity and optimized fidelity is plotted over pulse length in fig. 4.2. The optimizations where the fidelity goal was not reached, pulse lengths equal to and below 10.50 ns, are marked with stars.

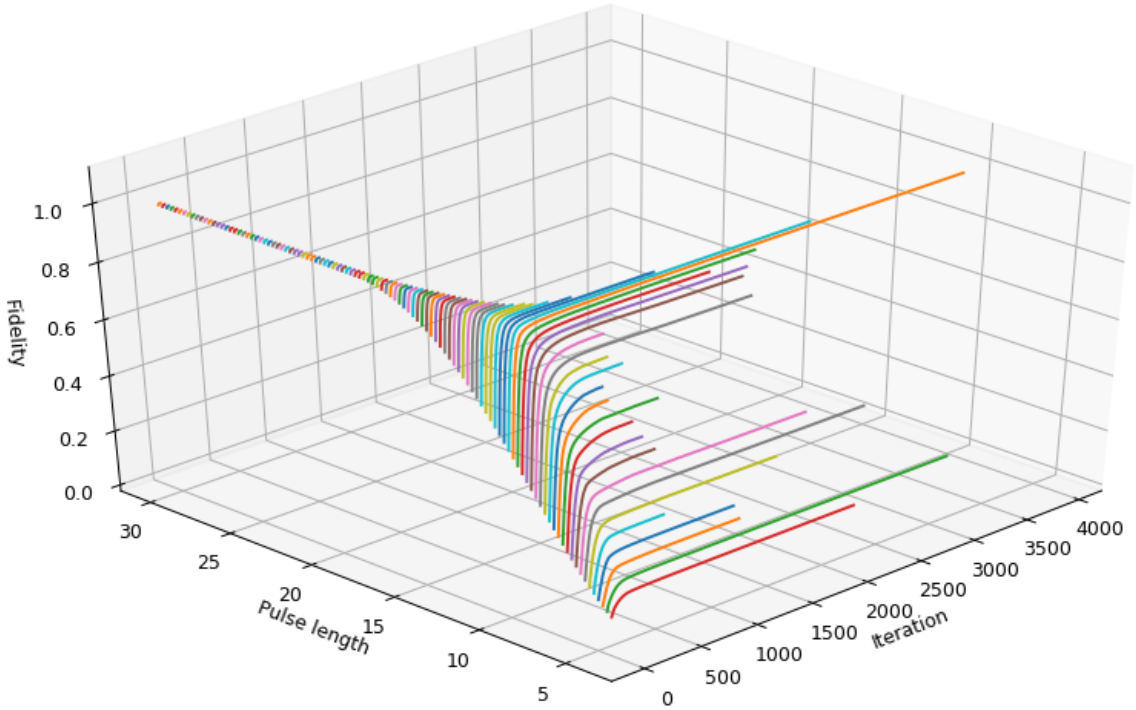

Figure 4.1: Fidelity during optimizations for every pulse length (ns). The different colors help distinguish the lines.

Further analysis is done on pulses with lengths 4.25 ns, 6.0 ns, 8.0 ns, 10.0 ns, 20.0 ns and 30.0 ns. The optimized pulse shapes $\mathrm{Re}(\Omega)$ and $\mathrm{Im}(\Omega)$ are plotted in fig. 4.3 together with the guess pulses. Pulses longer than 20 ns require only fine adjustments to the Blackman guess pulse while shorter pulses have an imaginary part which is maximized for the whole duration of the pulse.

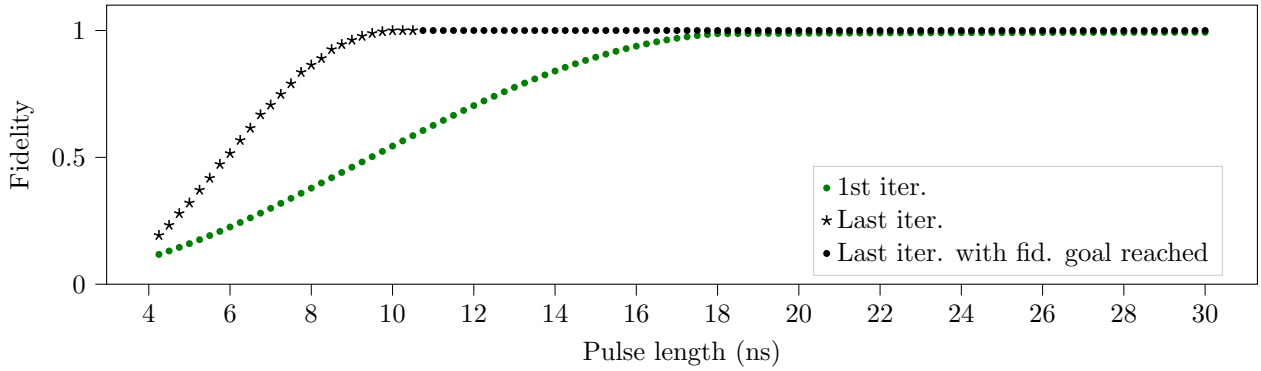

Figure 4.2: Fidelity of first and last iteration of every pulse length.

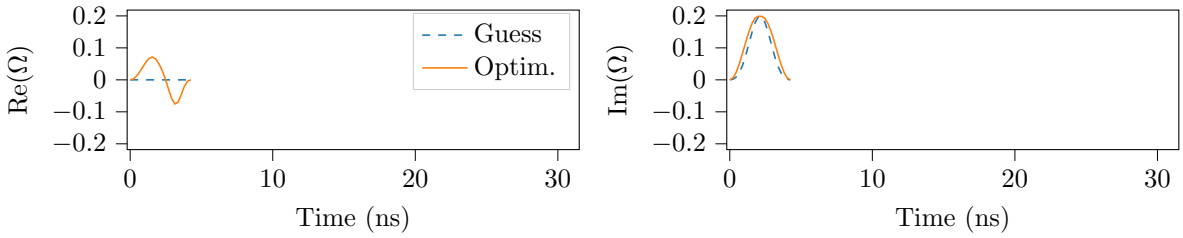

(a) Pulse length 4.25 ns

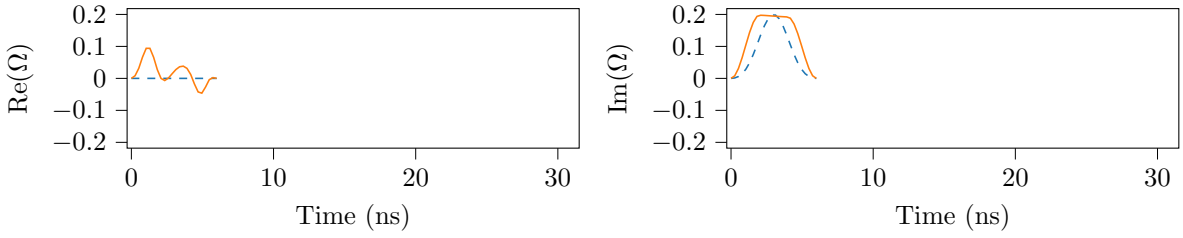

(b) Pulse length 6.0 ns

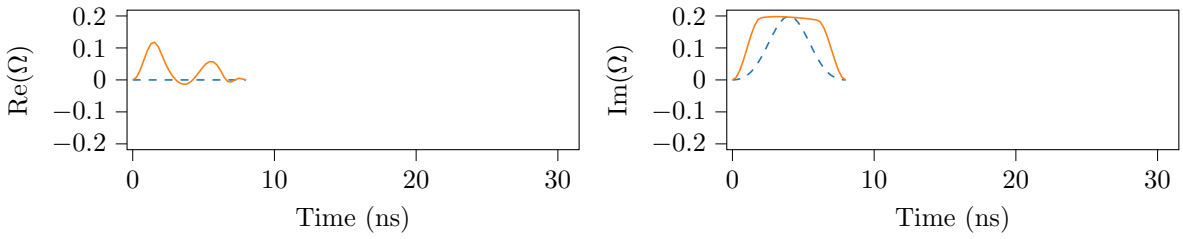

(c) Pulse length 8.0 ns

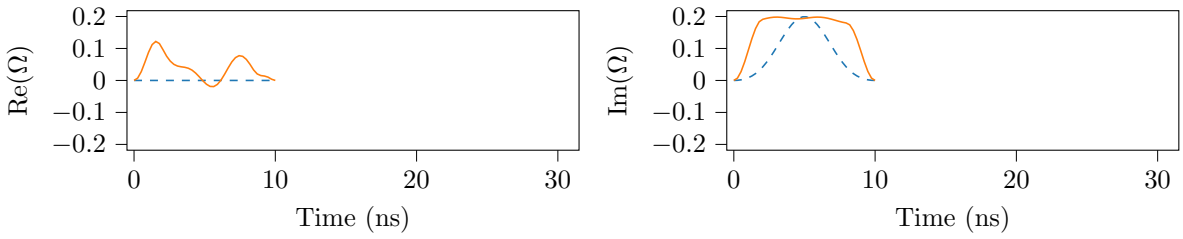

(d) Pulse length 10.0 ns

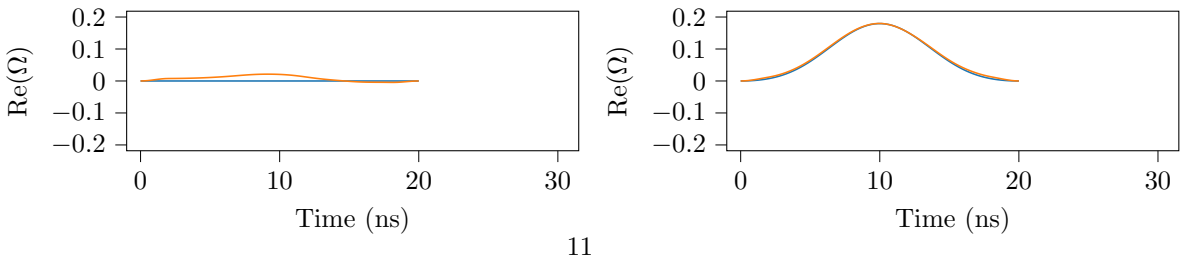

(e) Pulse length 20.0 ns

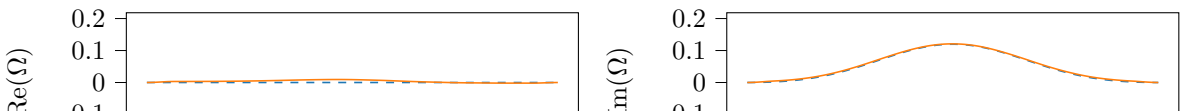

The spectrum of $\Omega(t)$ in the lab frame ($\Omega(t)e^{i\omega_q t}$) is shown in fig. 4.4. For all pulse lengths there is a peak centered roughly at ω_q with a quickly decaying end in positive direction (towards $\omega_q + \kappa_q$). Following the trend, it can be observed that the width of the peak becomes narrower for longer pulses. For the highest pulse length 30 ns there is almost no support at $\omega_q + \kappa_q$ nor $\omega_q - \kappa_q$.

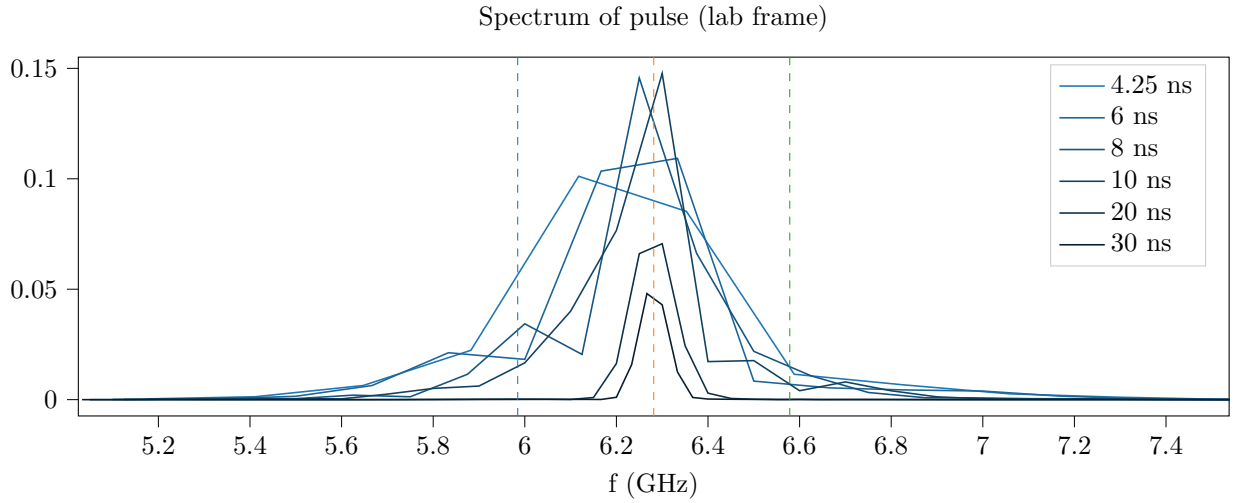

Figure 4.4: Frequency spectrum of the complex pulses in fig. 4.3. The vertical lines indicate (from left to right) $\omega_q - \kappa_q$, ω_q, $\omega_q + \kappa_q$ (all divided by 2π).

The time evolution of the system under the optimized pulses are visualized by plotting the occupation of the states over time, fig. 4.5, and the projection of the state on the Bloch sphere over time, fig. 4.6.

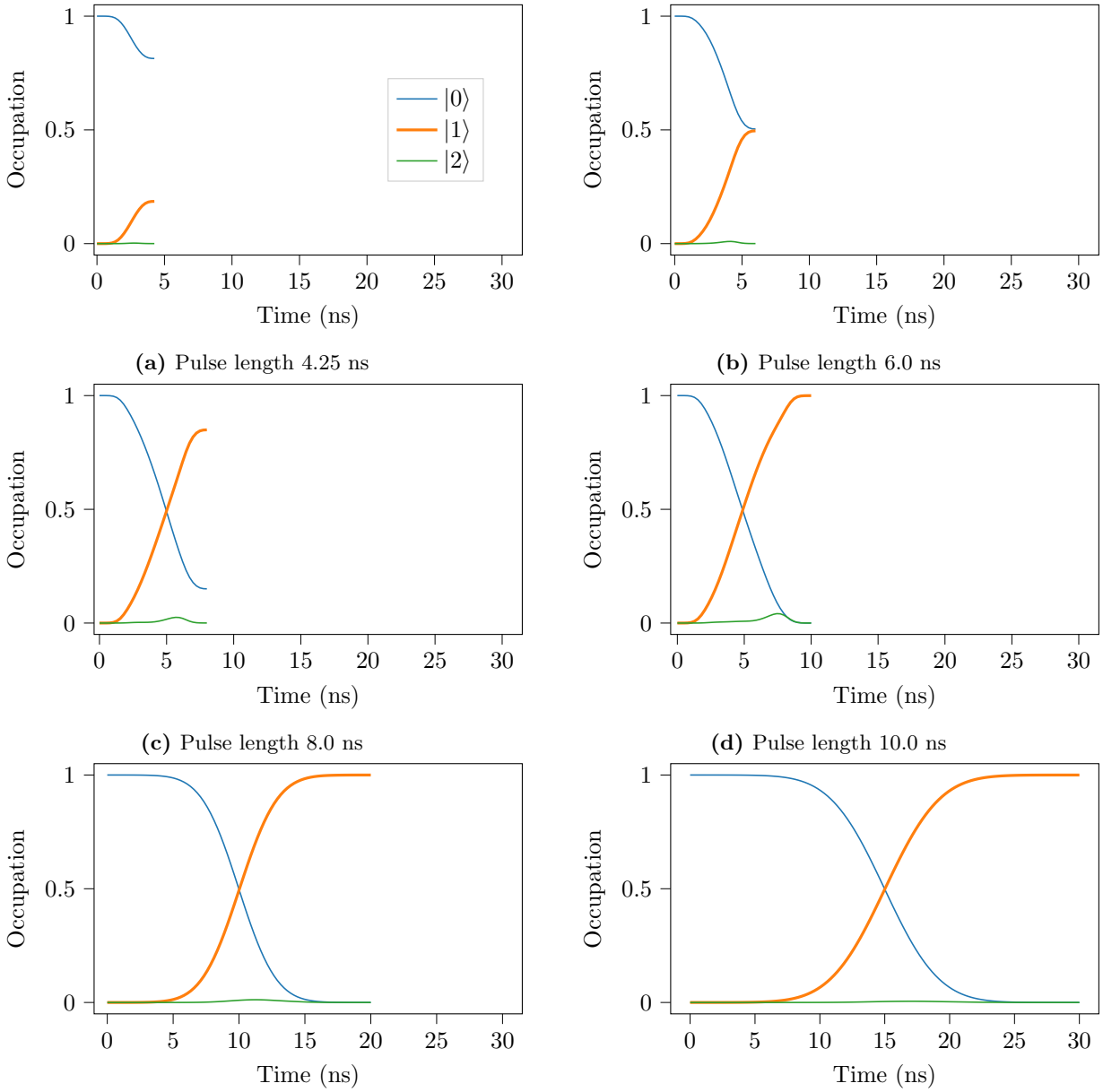

(a) Pulse length 4.25 ns

(b) Pulse length 6.0 ns

(c) Pulse length 8.0 ns

(d) Pulse length 10.0 ns

(e) Pulse length 20.0 ns

(f) Pulse length 30.0 ns

Figure 4.5: Energy level occupation over time for different lengths of optimized pulses.

For short pulse lengths there is not enough time for the transfer from $|0\rangle$ to $|1\rangle$, but for a pulse length of roughly 10.0 ns the goal is reached. Figure 4.5 **(b)** shows a little rise in occupation of $|2\rangle$ around 7.5 ns.

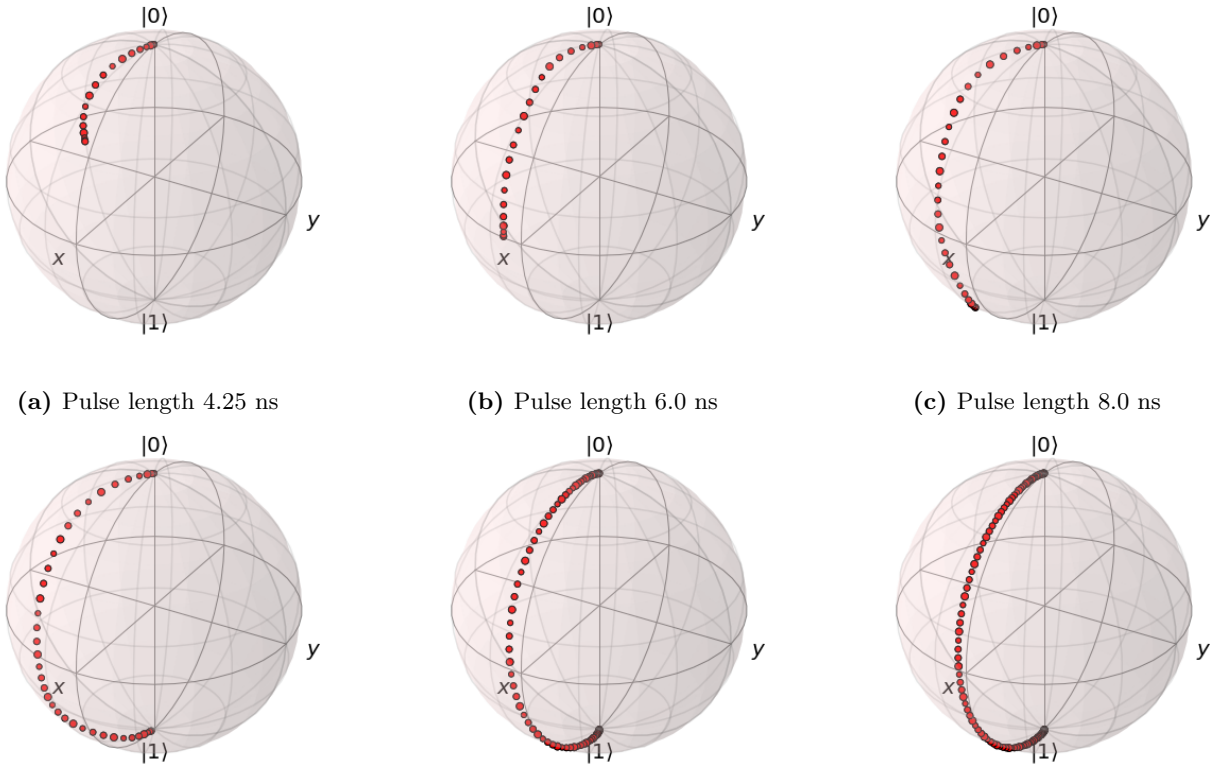

(a) Pulse length 4.25 ns **(b)** Pulse length 6.0 ns **(c)** Pulse length 8.0 ns

(d) Pulse length 10.0 ns **(e)** Pulse length 20.0 ns **(f)** Pulse length 30.0 ns

Figure 4.6: Time dynamics on the Bloch sphere for different lengths of optimized pulses.

From the Bloch sphere visualization it appears that shorter pulse lengths lead to deviations from the pure y-axis rotation. This can be clearly seen in fig. 4.6 **(d)** for a pulse length of 10 ns, where the fidelity goal was reached but short enough that the maximum amplitude is reached for the guess pulse.

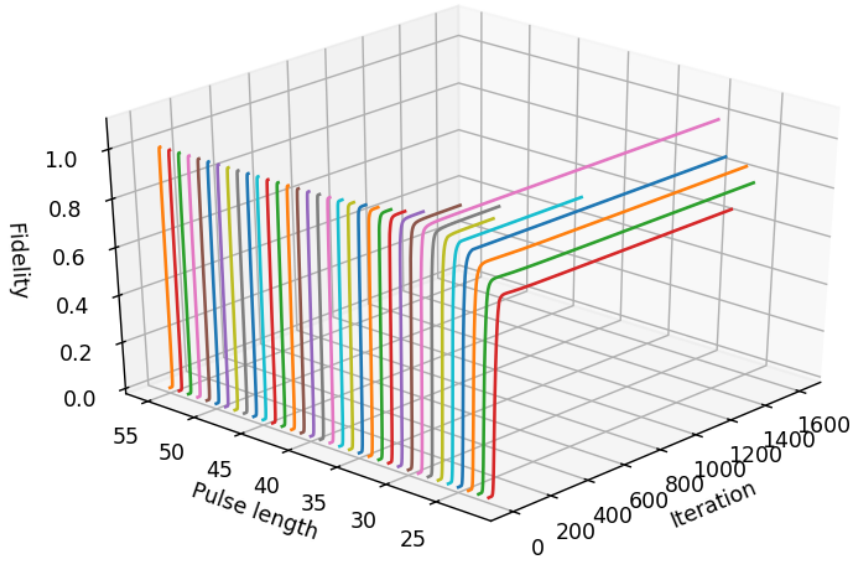

Figure 4.7: Fidelity during optimizations for every pulse length (ns).

4.1.2 $|0\rangle \rightarrow |2\rangle$ state transfer

Once again all optimization runs are shown in fig. 4.7. All runs start at almost zero fidelity while pulse lengths from 30 ns and up reach the fidelity goal of $F > 0.99999$. The number of iterations are relatively low down to 30 ns and for shorter pulses the iterations fluctuate. Note that for pulse lengths shorter than 22 ns the optimization stopped after the first iteration due to $\Delta F < 10^{-9}$.

In fig. 4.8 the fidelity is shown with respect to pulse length and here it is seen that the fidelity goal is reached for pulses down to 30 ns.

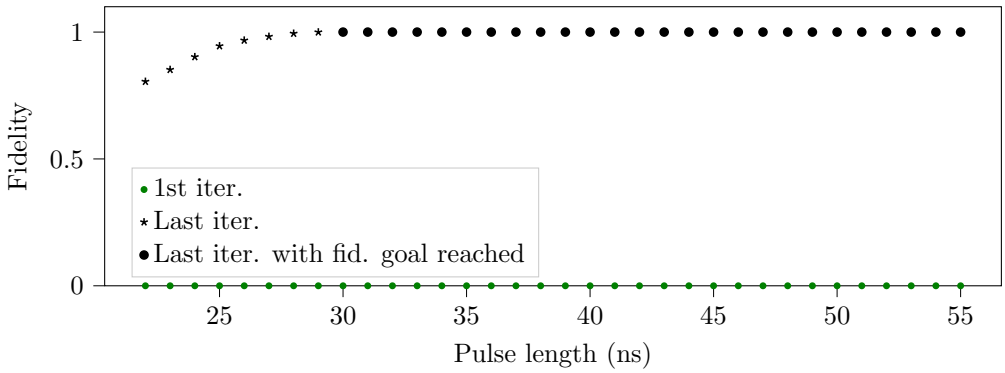

Figure 4.8: Fidelity of first and last iteration of every pulse length.

The optimized pulses are shown in fig. 4.9. For all pulse lengths the pulses have roughly the same shape with a quick rise and a short plateau, then oscillations until the end. The longest pulse at 55 ns has more oscillations than, but instead they are lower in amplitude. To get some insight, the frequency spectrum, fig. 4.10, shows large support at ω_q and $\omega_q + \kappa_q$, while for longer pulses a peak at $\omega_q - \kappa_q$ disappears. Just as the previous state transfer, the peaks narrow for longer pulse lengths.

The occupation dynamics in fig. 4.11 show a slow oscillation in all pulse lengths for all states. Further, the occupation probability of $|1\rangle$ rises to about 0.75 until the middle-point of the pulse and then falls to zero in the end, while $|2\rangle$ starts to rise at the point of the population inversion. For the shorter pulse lengths it can be seen that there isn't enough time to realise the transfer.

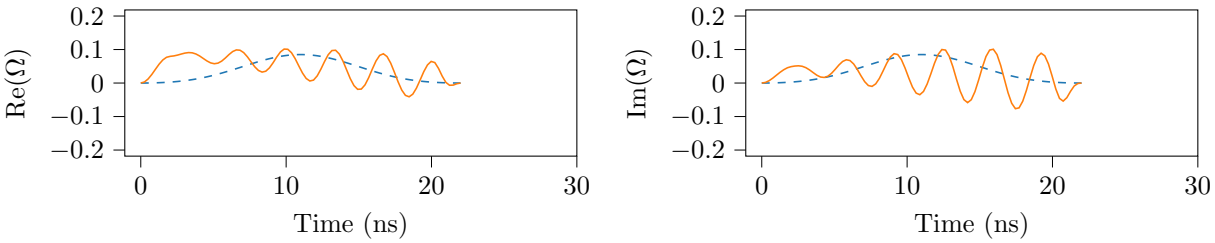

(a) Pulse length 22.0 ns

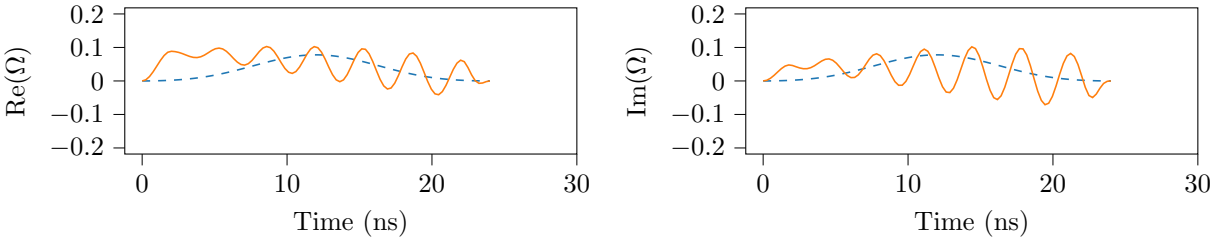

(b) Pulse length 24.0 ns

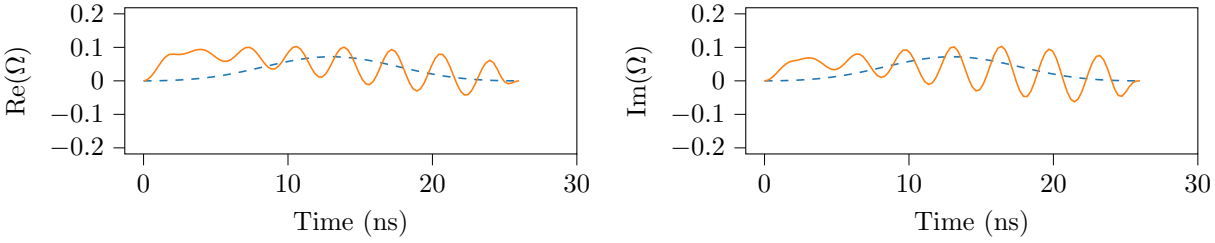

(c) Pulse length 26.0 ns

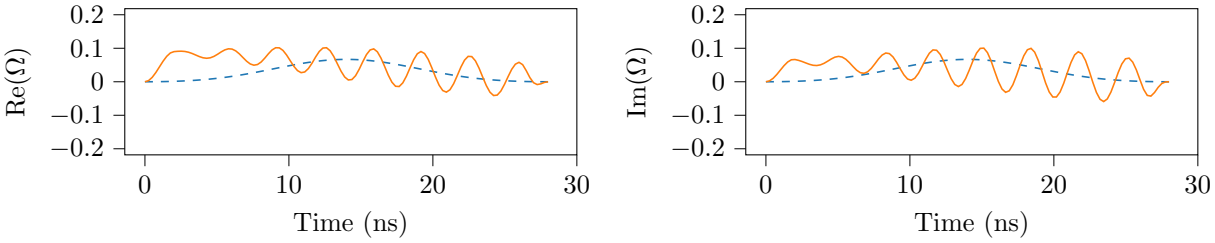

(d) Pulse length 28.0 ns

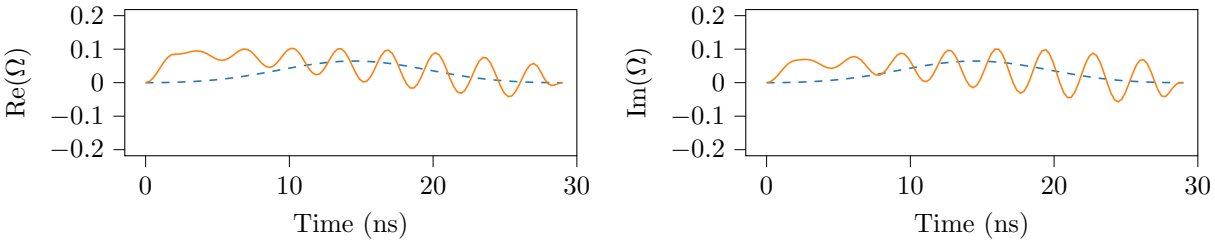

(e) Pulse length 29.0 ns

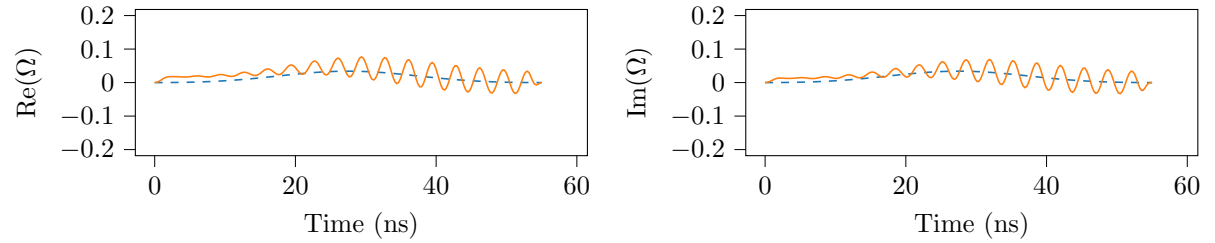

(f) Pulse length 55.0 ns

Figure 4.9: Optimised pulse shapes and guess pulses (dashed) for pulse lengths **(a)** 22 ns, **(b)** 24 ns, **(c)** 26 ns, **(d)** 28 ns, **(e)** 29 ns, and **(f)** 55 ns. Oscillations appear in all solutions.

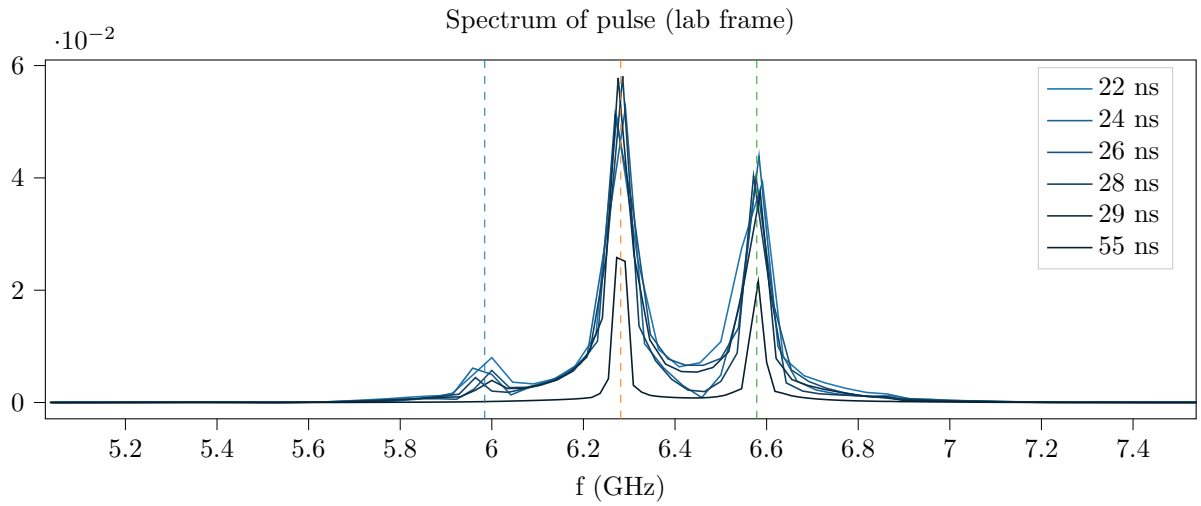

Figure 4.10: Frequency spectrum of the complex pulses in fig. 4.9. The vertical lines indicate (from left to right) $\omega_q - \kappa_q$, ω_q, $\omega_q + \kappa_q$ (all divided by 2π).

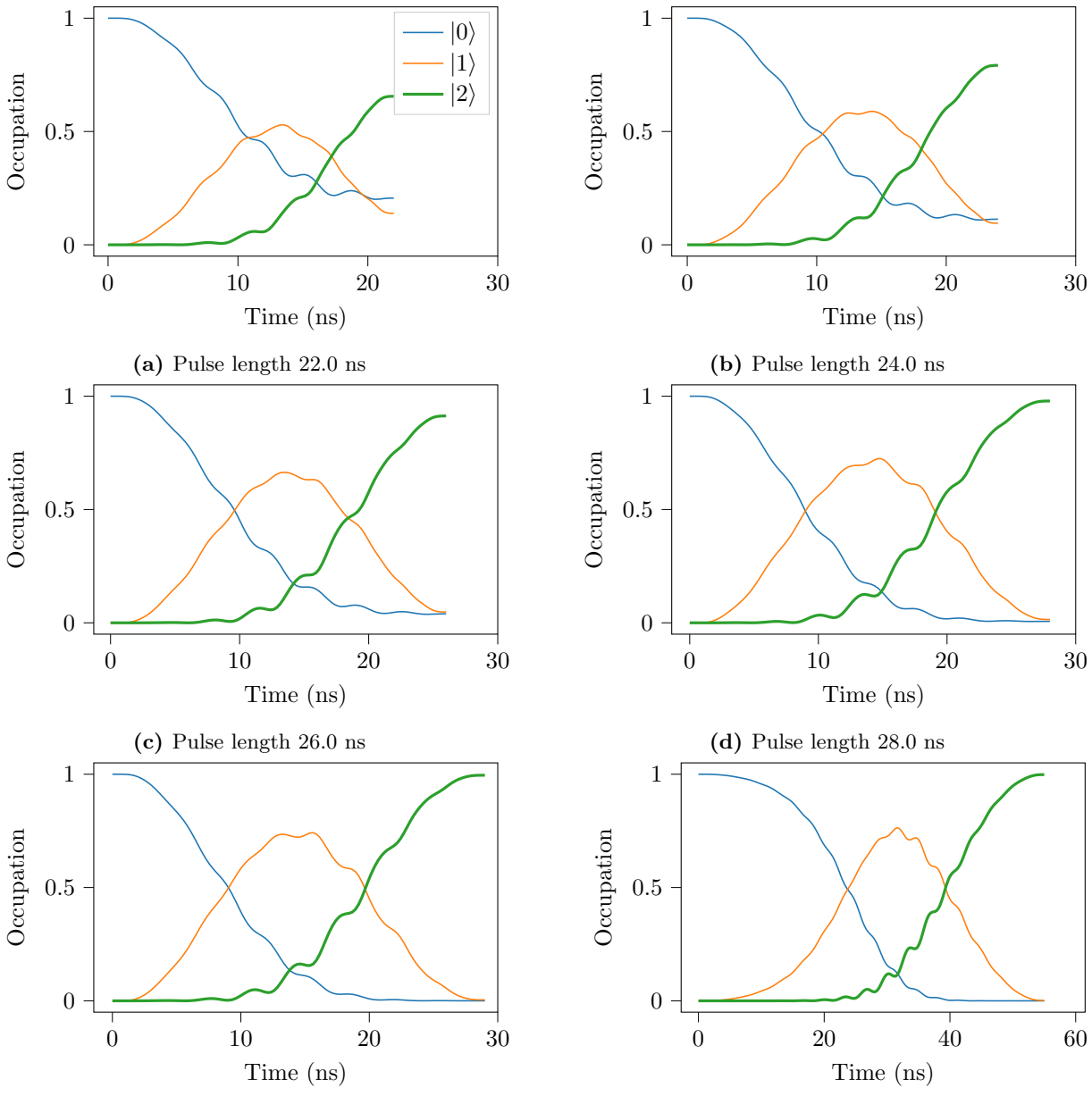

(a) Pulse length 22.0 ns

(b) Pulse length 24.0 ns

(c) Pulse length 26.0 ns

(d) Pulse length 28.0 ns

(e) Pulse length 29.0 ns

(f) Pulse length 55.0 ns

Figure 4.11: Energy level occupation over time for different lengths of optimized pulses.

4.2 Cat code encoding

The cat encoding optimization reached the convergence criteria of $\Delta F < 10^{-6}$ after 2389 iterations (totalling at roughly 41 hours and 28 minutes) with a fidelity $F = 0.999380$, (recall the fidelity measure for multiple objectives in eq. (3.1)). The individual fidelities for the 6 initial states are shown in table 4.1, where we can see that all individual fidelities are above 0.999000.

Table 4.1: Fidelities for the individual state transfers (ordered from highest to lowest).

State	F
$(\|0\rangle - \|1\rangle)/\sqrt{2}$	0.999553
$(\|0\rangle + i\,\|1\rangle)/\sqrt{2}$	0.999411
$(\|0\rangle + \|1\rangle)/\sqrt{2}$	0.999363
$\|0\rangle$	0.999362
$\|1\rangle$	0.999320
$(\|0\rangle - i\,\|1\rangle)/\sqrt{2}$	0.999272

The pulse shapes of the qubit and resonator are shown in fig. 4.12. Comparing the resonator and qubit we can see that the resonator pulse has rapid oscillations throughout the whole pulse while the qubit exhibits some small quick oscillation at sparse times. The spectrum of the pulse is shown in **??** and gives us some insight into the pulse shapes. The qubit control pulse shows a wide peak at ω_q, two small peaks at ω_r and $2\omega_r - \omega_q$ and two barely noticable peaks at $\frac{1}{4}\omega_r$ and $\frac{1}{2}\omega_r$. The resonator pulse has one wide peak at ω_r, a smaller one at ω_q and an even smaller peak at $2\omega_r - \omega_q$.

The dynamics of the qubit is shown in fig. 4.14 for all state transfers. Here we see that there is always a rapid oscillation present in the occupation probability. Looking at the dynamical behaviour one can see that common for all transfers is for the qubit to stay somewhat close to an equal superposition between $|0\rangle$ and $|1\rangle$ and then at circa 50 ns evolve to $|0\rangle$.

One interesting measure we can look at is the maximum occupation of the 8 resonator states. This can give us information about the the validity of the Hilbert space truncation. In fig. 4.15 the maximum reached occupation probability are plotted for all states. This is done for all the 6 state transfers. Looking only at the odd states there is a clear downward trend for higher states, with $|7\rangle$ only reaching circa 0.2 of occupation probability during the $|0\rangle$ transfer. $|6\rangle$ is in the 0.2–0.3 occupation range for all transfers. The dynamics of the resonator are provided in appendix A.2 for further analysis.

Finally we can plot the Wigner function of the final resonator states and compare it with the target states. This is done in fig. 4.16 where the final states have been transformed back into the lab frame. As is evident from the plots they are close to the target states shown in fig. 2.3.

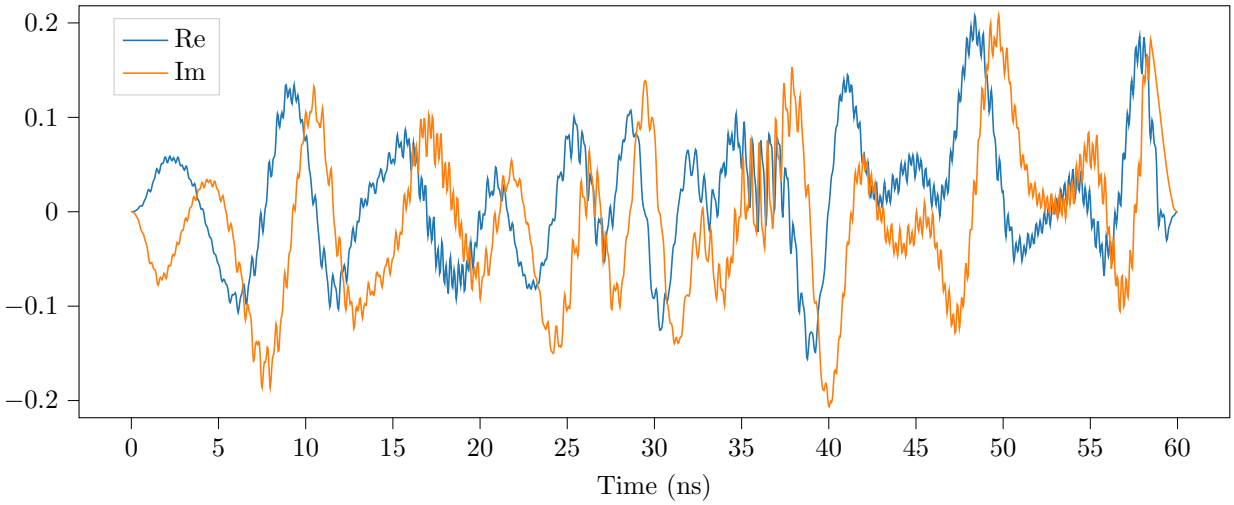

(a) Qubit control pulse shape.

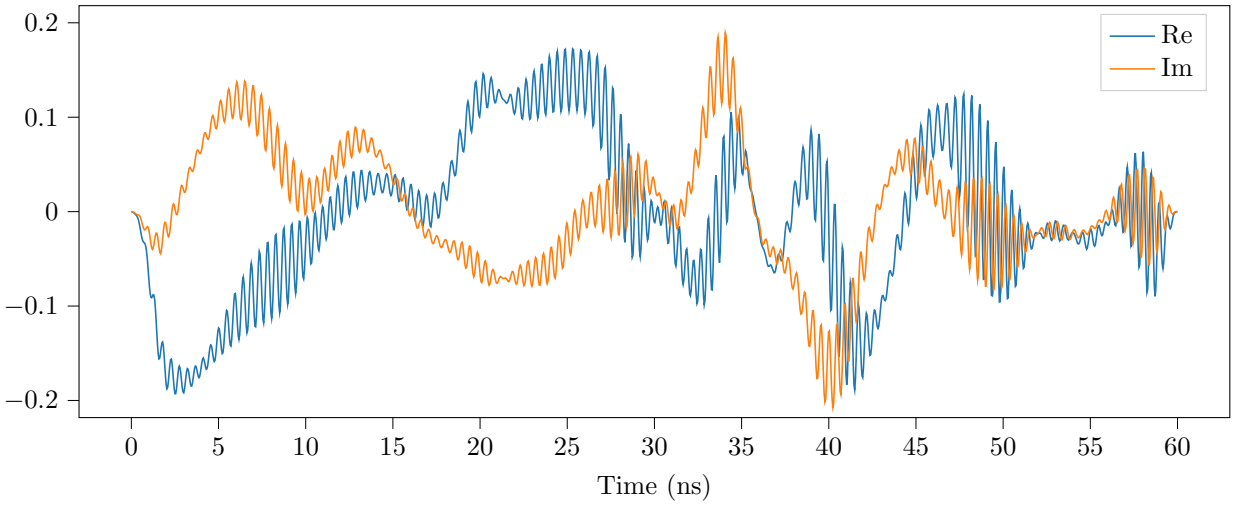

(b) Resonator control pulse shape.

Figure 4.12: Optimized pulse shapes of **(a)** $\Omega_q(t)$ and **(b)** $\Omega_r(t)$. The real and imaginary parts of the pulse are shown in blue and orange respectively. The resonator shows rapid oscillations compared to the qubit.

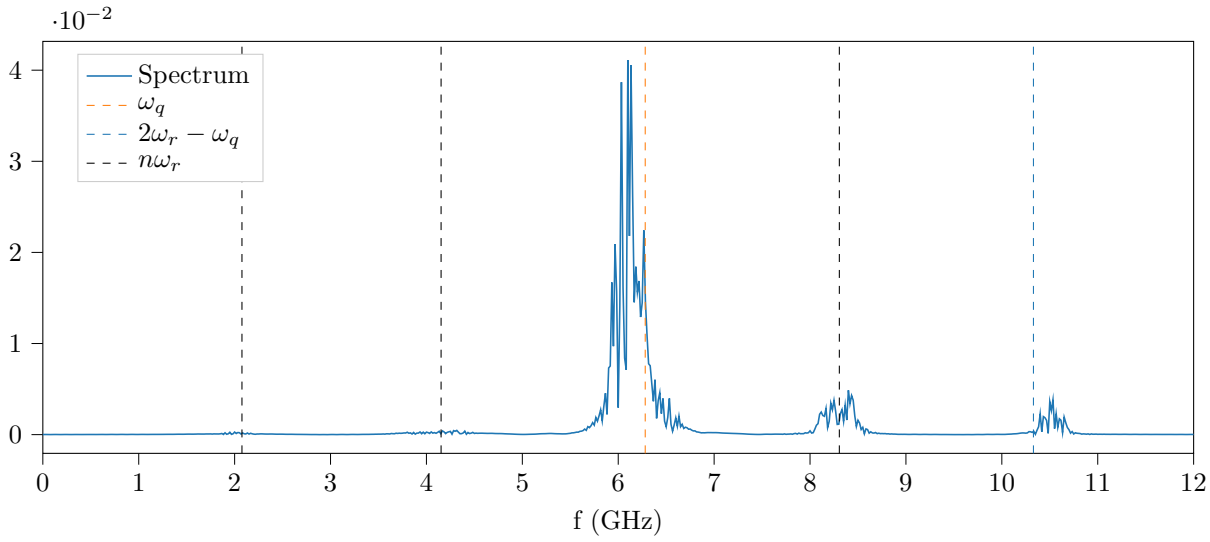

(a) Qubit control pulse spectrum. The black vertical are located at $n\omega_r$ where $n = (0.25, 0.5, 1)$.

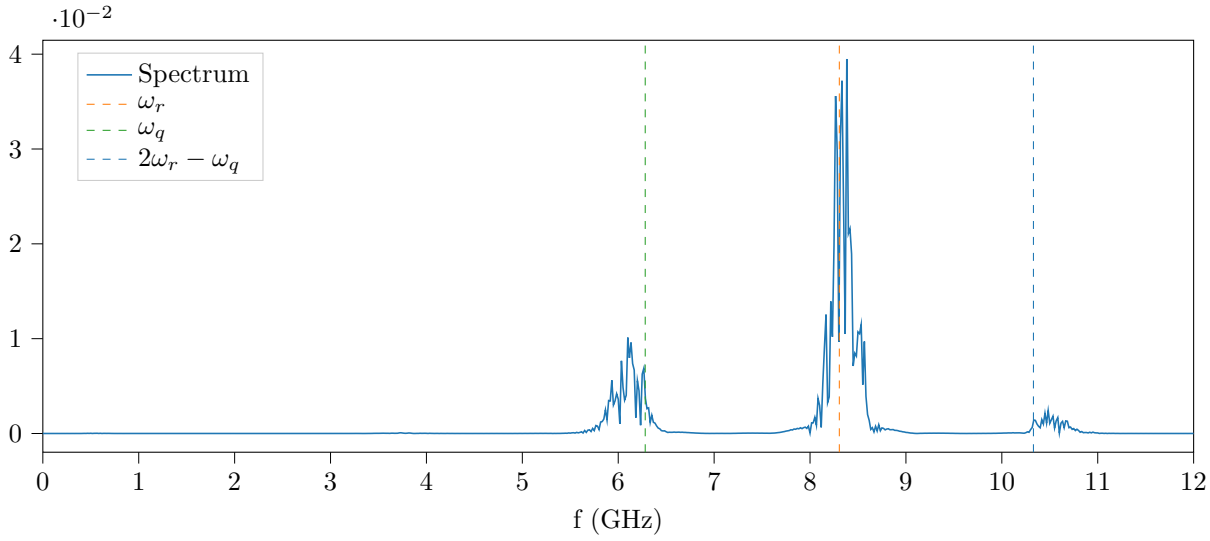

(b) Resonator control pulse spectrum.

Figure 4.13: Spectrum of optimized pulses **(a)** $\Omega_q(t)$ and **(b)** $\Omega_r(t)$ (in the lab frame).

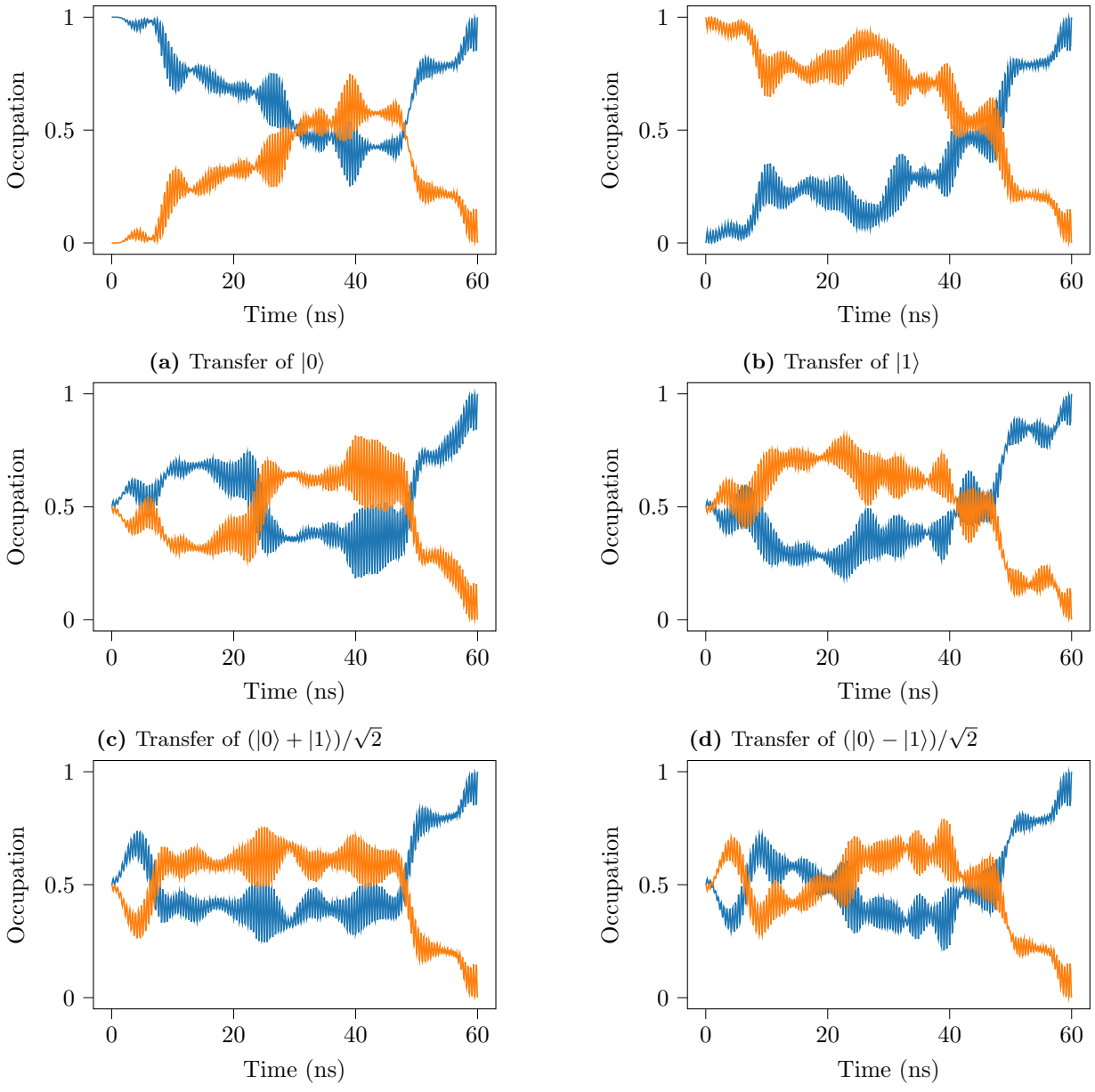

(a) Transfer of $|0\rangle$

(b) Transfer of $|1\rangle$

(c) Transfer of $(|0\rangle + |1\rangle)/\sqrt{2}$

(d) Transfer of $(|0\rangle - |1\rangle)/\sqrt{2}$

(e) Transfer of $(|0\rangle + i\,|1\rangle)/\sqrt{2}$

(f) Transfer of $(|0\rangle - i\,|1\rangle)/\sqrt{2}$

Figure 4.14: Qubit level occupation over time for the 6 state transfers. $|0\rangle$ and $|1\rangle$ are shown in blue and orange respectively.

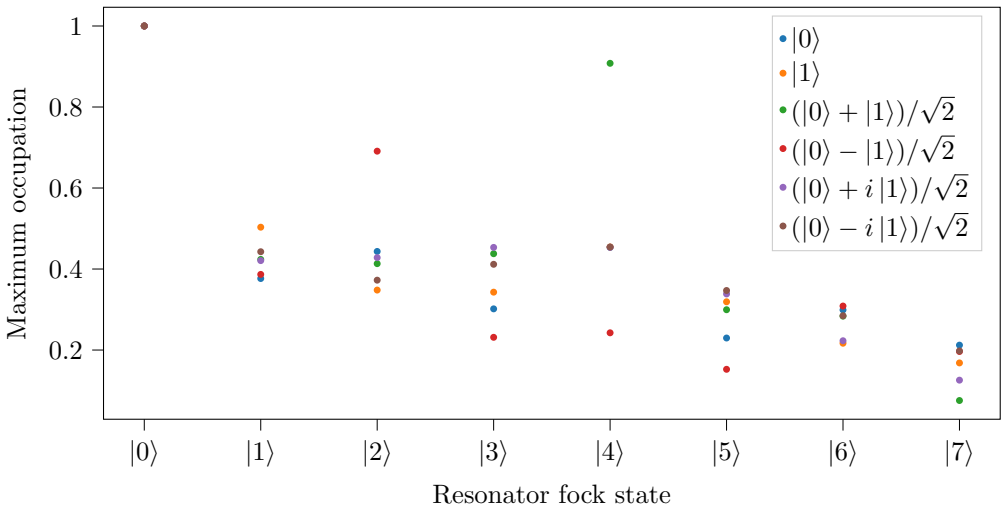

Figure 4.15: asda

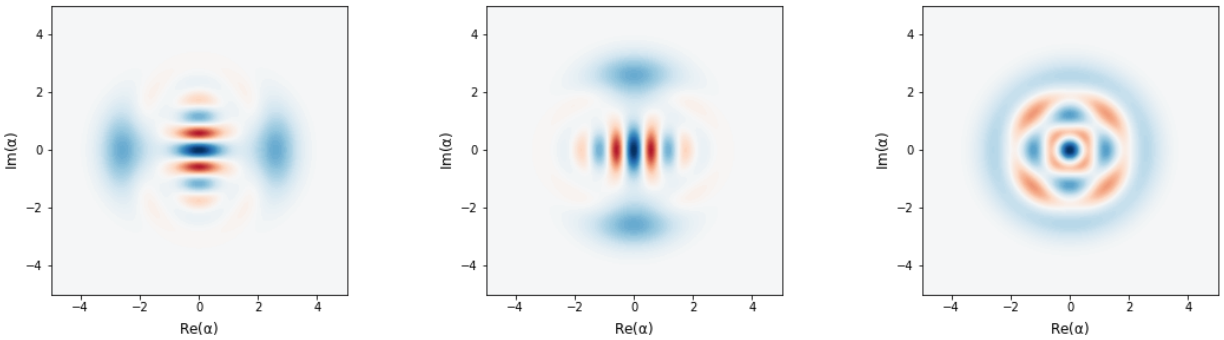

(a) Transfer of $|0\rangle$ **(b)** Transfer of $|1\rangle$ **(c)** Transfer of $(|0\rangle + |1\rangle)/\sqrt{2}$

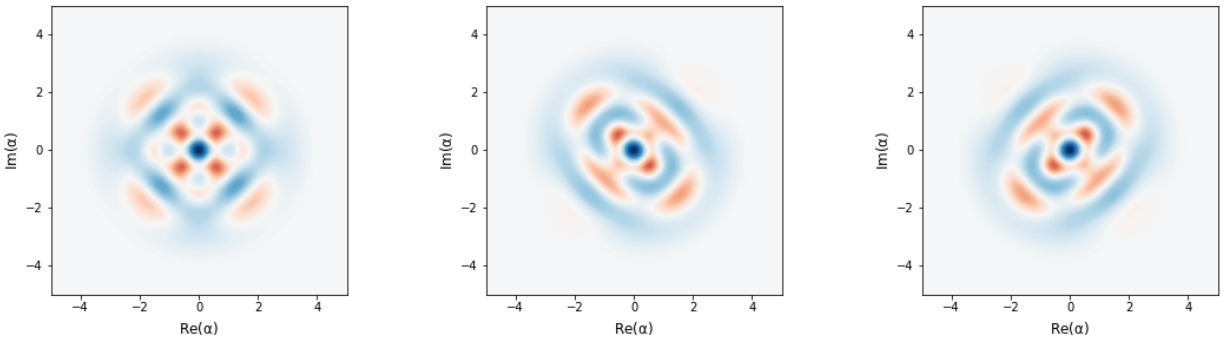

(d) Transfer of $(|0\rangle - |1\rangle)/\sqrt{2}$ **(e)** Transfer of $(|0\rangle + i\,|1\rangle)/\sqrt{2}$ **(f)** Transfer of $(|0\rangle - i\,|1\rangle)/\sqrt{2}$

Figure 4.16: Wigner function of final state (lab frame) of the resonator for all state transfers. The final resonator states are close to the target states shown in fig. 2.3.

5 Discussion

In this chapter the methods, results and analyses will be discussed, first for the qubit state transfers and secondly for the cat code encodings.

5.1 Qubit State Transfers

We start by looking at the $|0\rangle \rightarrow |1\rangle$ transfer. As the system was set up to realise a π-rotation for a Blackman pulse with length $T = 6\sigma = 6 \times 3\,\text{ns} = 18\,\text{ns}$, it is no suprise that the starting fidelity is almost unity down to pulse lengths of 18 ns. Shorter than that, the amplitude constraint affects the starting pulse; it is maximised but starts to become shorter. This explains the drop in starting fidelity all the way down to 4.25 ns. Further, for pulse lengths shorter than 10.75 ns the optimization cannot reach the fidelity goal of $F > 0.99999$ which is expected as the amplitude constraint means that there just is not enough time to realise the state transfer. This is supported by the fact that the imaginary part is maximised for pulse lengths shorter than 10.75 ns. It can be assumed that the optimization is trying to compensate for the shorter pulse time.

One possible reason for the fluctuations in the number of iterations for the pulse lengths which did not reach the fidelity goal is that the steepness around the (assumed) local minima could differ significantly from each other. This is very much in contrast to the low and steady number of iterations needed when the fidelity goal is reached. Even though the increase in pulse length should increase the number of possible solutions, increasing the chance of reaching the fidelity goal, the fast convergence is most probably due to the fact that the initial guess pulse brings the state so close to the target. One might consider exploring this solution space, however it could potentially be infinite in size. This is not needed to use the optimized pulse shapes as any solution which realises the transfer should be good enough.

With the previous statement in mind, the fact that the solutions found for pulse lengths shorter than 18 ns show a small increase in the $|2\rangle$ population after the population inversion could point to a need to penalize this state. That is because if the state is too occupied during the transfer one cannot be sure that the states above that will remain unoccupied. This could be checked by simulating the system using the optimized pulses, but with a larger Hilbert space. If the final state reaches the target, the truncation is a good approximation. `krotov` suggests to add dissipation to the states which should be penalized as there is currently no support for state-dependent constraints. However this also increases the computation time as the Hamiltonian needs to either be expressed as a Liouvillian or propagated with collapse terms in the master equation.

The spectrum of the pulse shapes somewhat explains the "strategy" of the optimization. For the longer pulse lengths there is no problem in keeping the pulse frequency mostly around the first transition frequency, only driving the qubit to $|0\rangle$. As the pulses become shorter the peak becomes wider, but the solutions try to keep the amplitude at the second transition frequency $\omega_r + \kappa_q$ low to keep the qubit from going into $|2\rangle$. Eventually for short enough pulses this level becomes a little bit occupied, as stated before, but then drops to zero. Perhaps the solution tries to "take a shortcut" through $|2\rangle$, which may be a viable strategy, but if that is the case then one needs to set $N_q = 4$ and penalize $|3\rangle$ to make sure that the truncation is a valid approximation.

In conclusion, `krotov` has no problem finding a solution to this simple state transformation. Now we continue with the $|0\rangle \rightarrow |2\rangle$ transfer. The "strategy" for all pulse lengths in this case is to first invert the population and then at the halfway point start simultaneously driving the second transition level to start pumping to $|2\rangle$. The pulse shapes also reflects this as the oscillation that starts after the plateau has a frequency of κ_q, which is also visible in the frequency spectrum. While the peak at $\omega_q + \kappa_q$ was expected, the peak at $\omega_q - \kappa_q$ for pulse lengths shorter than 29 ns is a suprise with no clear explanation as to why. It is also not clear why the solutions drive harder at this frequency the shorter the pulse length.

For this optimization the initial guess pulses were very far from any solution, with the fidelity almost starting at zero for all pulse lengths. The fidelity goal $F > 0.99999$ was reached down to $T = 30\,\text{ns}$ which is a bit longer than the $|0\rangle \rightarrow |1\rangle$ transfer. Looking at the occupation dynamics and pulse shapes could give a clue as to why this is the case. One reason could be that there needs to be enough periods of oscillations to drive to $|2\rangle$, which is not the case for the $|0\rangle \rightarrow |1\rangle$ transfer where the integral of the pulse shape is of importance. Further, it appears that the fidelity drops in the same way as the $|0\rangle \rightarrow |1\rangle$ transfer for shorter pulse lengths. However we cannot draw any conclusions for pulse lenghts shorter than 22 ns. Perhaps with a low ΔF one might reach a solution that follows the trend, but this is only speculation.

The number of iterations also fluctuate for pulse lengths which don't reach the fidelity goal, just as the $|0\rangle \rightarrow |1\rangle$ transfer.

Interestingly, for both transfers the optimization converges quickly to a relatively high fidelity while the majority of the time is spent fine-tuning the pulse shapes. This could be a side-effect of the static step size. While the number of iterations were large, each iteration step was faster than 1 second, so the total optimization might not be a problem. This optimization time could potentially grow exponentially for larger Hilbert spaces though.

To conclude, `krotov` can also be used to optimize for somewhat more complicated transfers than the simple qubit rotation.

5.2 Cat code encoding

The 6 simultaneous objective optimization ended with a total fidelity of $F = 0.999380$ and the individual fidelities all over $F > 0.999000$. This supports the validity of the method as a means to obtain one pulse to encode all 6 states. Even though the fidelity goal of $F > 0.999999$ was not reached it could be possible to reach by decreasing ΔF. Note however that there is no guarantee that such a solution exists. To continue, the differences in the individual fidelities are most probably due to numerical instability as they are very small.

Looking at the pulse shapes, fig. 4.12, doesn't give much insight however the spectrum shows some interesting phenomena. The qubit control pulse spectrum shows a large peak at the qubit resonance frequency ω_q, as expected, and the same with the resonator and its' resonance frequency ω_r. However there is no clear explanation for the peak at $2\omega_r - \omega_q$ and the peaks of the resonator appearing in the qubit spectrum and vice versa. The width of the resonance peaks for the qubit (resonator) could perhaps be explained by the resonator (qubit) inducing a resonance shift dependent on the state of the qubit (resonator). Consequently, during different times of the pulse the system needs to be driven at a range of frequencies. Further research is needed to explain the characteristics of the solution.

The only discernable "strategy" found, judging by the qubit dynamics in fig. 4.14, is to put the qubit in a superposition which will drive the resonator into the desired state using the coupling. This is in line with the strategy presented in **quantum dynamics**. However, further analysis of the resonator and qubit dynamics and interactions could bring a further understanding.

One significant issue with the final state is that it is not that robust with respect to small changes in the pulses, as can be seen from the fact that the fidelity goal is reached in the last fraction of a nanosecond. This could be due to the relatively large coupling factor g which was chosen as to allow for a shorter total pulse length. The large coupling will force the qubit and resonator to induce oscillations in each other. However even though decreasing this would help mitigate the problem this would require a longer pulse length and therefore longer computation times (as the time step is fixed). The proposed solution is to add a mechanism for optimizing pulse shapes with points sparser than the time grid, and also enable time-dependent Hamiltonians to be used, with arbitrary initial phase shifts. As the `krotov` package already provides a way to optimize ensemble objectives with different parameters in each Hamiltonian [15] for robustness, this could be used to optimize for the average of the added phase shift. This should give more robust pulses.

As the previous experiments showed that `krotov` could optimize simple non-coupled qubits (resonators) with a high fidelity and reasonable physical intuition, this gives support to the validity of the cat code encoding pulses. Even though the underlying theory of the solution is not understood at this moment, Krotov's method proves itself to be able to optimize a state transfer in a qubit-resonator coupled system to a fidelity $F > 0.9990$. Further experiments need to be done to assess the performance of the pulses in a physical environment, such as including noise which is a significant factor.

5.3 General discussion of `krotov`

`krotov` provides an easy-to-use interface for setting up the optimization problem. This is the strongest argument for using this package as the features are unrivaled compared to other optimization packages. Firstly, QuTiP [14] can optimize with the GRAPE and CRAB algorithms, but there are no provided interfaces for (1) saving optimizations to a file, (2) continuing optimization efter they are stopped, (3) optimizing for multiple control fields and objectives, (4) using custom convergence criteria and (5) modifying the pulses after every iteration (for amplitude constraints). These are critical features which `krotov` has. Secondly, GOAT [16] is a new promising algorithm for quantum optimal control, but has no Python package available yet and the MATLAB

implementation has a steep learning curve. If or when the GOAT Python implementation becomes available it would be interesting to compare the feature set and the actual algorithm by testing comparing the performance on the same optimization objective.

The slow convergence of the optimization could pose a problem for larger systems, however there are some techniques for speeding up the optimization which will be presented in section 6.2. If all else fails one could always throw more compute at it.

6 Conclusion

In conclusion, Krotov's method efficiently realises the $|0\rangle \rightarrow |1\rangle$ transfer for various pulse lengths when supplying guess pulses close to π-pulses. It can also find non-trivial solutions for shorter pulse lengths, when an amplitude constraints is present,

6.1 Using `krotov` For Cat Code Encoding Pulse Generation

Together with improvements in the model and techniques for speeding up the optimization this could be a valid tool in realising QEC with cat codes as the pulses only need to be found once in order to be used for encoding.

6.2 Future work

Improving the speed of the optimizations in this thesis could be done by

- parallelizing the simultaneous objectives (`krotov` provides an interface for this),
- using the dispersive regime approximation and
- implement a problem-specific system propagator using Cython.

Dispersive regime Penalize higher states Include dissipation (Liouvillian) Ensemble optimization for different phases of the coupling pulses

Perhaps one could find an optimization method that is faster at fine-tuning and combine this with Krotov's method.

References

[1] A. C. Santos, The IBM Quantum Computer and the IBM Quantum Experience, *Revista Brasileira de Ensino de Física* **39**, no. 1 Sep. 2016, Sep. 2016. DOI: 10.1590/1806-9126-RBEF-2016-0155. [Online]. Available: http://arxiv.org/abs/1610.06980 (visited on 05/10/2019).

[2] J. Preskill, Quantum Computing in the NISQ era and beyond, *Quantum* **2** Aug. 2018, 79, Aug. 2018. DOI: 10.22331/q-2018-08-06-79. [Online]. Available: http://arxiv.org/abs/1801.00862 (visited on 02/28/2019).

[3] D. Gottesman, An Introduction to Quantum Error Correction and Fault-Tolerant Quantum Computation, *arXiv:0904.2557 [quant-ph]* Apr. 2009, Apr. 2009. [Online]. Available: http://arxiv.org/abs/0904.2557 (visited on 05/10/2019).

[4] Z. Leghtas, G. Kirchmair, B. Vlastakis, R. J. Schoelkopf, M. H. Devoret, and M. Mirrahimi, Hardware-Efficient Autonomous Quantum Memory Protection, *Physical Review Letters* **111**, no. 12 Sep. 2013, 120501, Sep. 2013. DOI: 10.1103/PhysRevLett.111.120501. [Online]. Available: https://link.aps.org/doi/10.1103/PhysRevLett.111.120501 (visited on 05/10/2019).

[5] M. Mirrahimi, Z. Leghtas, V. V. Albert, S. Touzard, R. J. Schoelkopf, L. Jiang, and M. H. Devoret, Dynamically protected cat-qubits: A new paradigm for universal quantum computation, *New Journal of Physics* **16**, no. 4 Apr. 2014, 045014, Apr. 2014. DOI: 10.1088/1367-2630/16/4/045014. [Online]. Available: http://arxiv.org/abs/1312.2017 (visited on 01/29/2019).

[6] N. Ofek, A. Petrenko, R. Heeres, P. Reinhold, Z. Leghtas, B. Vlastakis, Y. Liu, L. Frunzio, S. M. Girvin, L. Jiang, M. Mirrahimi, M. H. Devoret, and R. J. Schoelkopf, Extending the lifetime of a quantum bit with error correction in superconducting circuits, English, *Nature; London* **536**, no. 7617 Aug. 2016, 441–445, Aug. 2016. DOI: http://dx.doi.org.proxy.lib.chalmers.se/10.1038/nature18949. [Online]. Available: http://search.proquest.com/docview/1815378608/abstract/D91F00AED7CC42E9PQ/1 (visited on 01/23/2019).

[7] N. Khaneja, T. Reiss, C. Kehlet, T. Schulte-Herbrüggen, and S. J. Glaser, Optimal control of coupled spin dynamics: Design of NMR pulse sequences by gradient ascent algorithms, *Journal of Magnetic Resonance* **172**, no. 2 Feb. 2005, 296–305, Feb. 2005. DOI: 10.1016/j.jmr.2004.11.004. [Online]. Available: http://www.sciencedirect.com/science/article/pii/S1090780704003696 (visited on 01/30/2019).

[8] D. M. Reich, M. Ndong, and C. P. Koch, Monotonically convergent optimization in quantum control using Krotov's method, *The Journal of Chemical Physics* **136**, no. 10 Mar. 2012, 104103, Mar. 2012. DOI: 10.1063/1.3691827. [Online]. Available: https://aip.scitation.org/doi/10.1063/1.3691827 (visited on 04/29/2019).

[9] M. H. Goerz, D. Basilewitsch, F. Gago-Encinas, M. G. Krauss, K. P. Horn, D. M. Reich, and C. P. Koch, Krotov: A Python implementation of Krotov's method for quantum optimal control, *arXiv:1902.11284 [quant-ph]* Feb. 2019, Feb. 2019. [Online]. Available: http://arxiv.org/abs/1902.11284 (visited on 03/13/2019).

[10] Y. Wu and X. Yang, Strong-Coupling Theory of Periodically Driven Two-Level Systems, *Physical Review Letters* **98**, no. 1 Jan. 2007, 013601, Jan. 2007. DOI: 10.1103/PhysRevLett.98.013601. [Online]. Available: https://link.aps.org/doi/10.1103/PhysRevLett.98.013601 (visited on 05/29/2019).

[11] Glosser.ca, *English: Bloch sphere; a geometrical representation of a two-level quantum system. Rendered with Asymptote.* Dec. 2012. [Online]. Available: https://commons.wikimedia.org/wiki/File:Bloch_Sphere.svg (visited on 05/22/2019).

[12] R. Fisher, "Optimal Control of Multi-Level Quantum Systems", Dissertation, Technische Universität München, München, 2010.

[13] D. d'Alessandro, *Introduction to quantum control and dynamics*. Chapman and Hall/CRC, 2007.

[14] J. R. Johansson, P. D. Nation, and F. Nori, QuTiP 2: A Python framework for the dynamics of open quantum systems, *Computer Physics Communications* **184**, no. 4 Apr. 2013, 1234–1240, Apr. 2013. DOI: 10.1016/j.cpc.2012.11.019. [Online]. Available: http://arxiv.org/abs/1211.6518 (visited on 05/28/2019).

[15] M. H. Goerz, E. J. Halperin, J. M. Aytac, C. P. Koch, and K. B. Whaley, Robustness of high-fidelity Rydberg gates with single-site addressability, *Physical Review A* **90**, no. 3 Sep. 2014, 032329, Sep. 2014. DOI: 10.1103/PhysRevA.90.032329. [Online]. Available: https://link.aps.org/doi/10.1103/PhysRevA.90.032329 (visited on 06/02/2019).

[16] S. Machnes, E. Assémat, D. J. Tannor, and F. K. Wilhelm, Gradient optimization of analytic controls: The route to high accuracy quantum optimal control, *Physical Review Letters* **120**, no. 15 Jul. 2015, Jul. 2015. DOI: 10.1103/PhysRevLett.120.150401. [Online]. Available: http://arxiv.org/abs/1507.04261 (visited on 03/14/2019).

A Appendix

A.1 Jupyter Notebooks and Optimization Data

To ease the reproducibility of the experiments the Jupyter notebooks used in this thesis and majority of resulting data are available at `https://github.com/JohanWinther/cat-state-encoding`. Although the project

A.2 Cat code resonator occupation

The occupation dynamics for the resonator are plotted in fig. A.1. Although they are hard to read and no conclusions are drawn from them in the thesis they are included in the appendix as reference for further analysis.

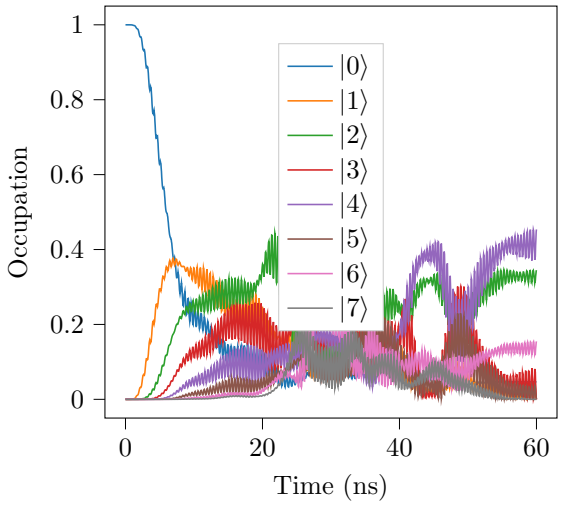

(a) Transfer of $|0\rangle$

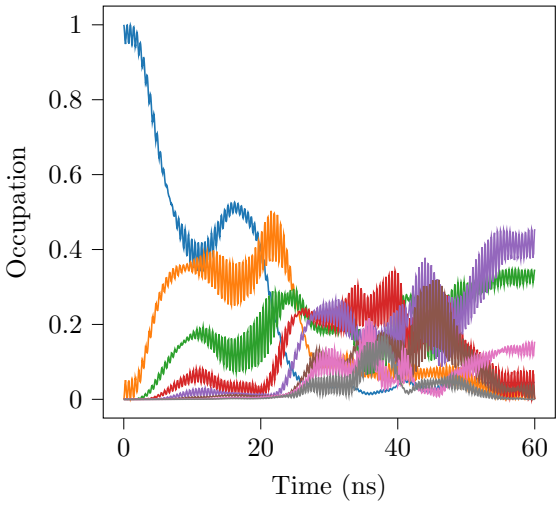

(b) Transfer of $|1\rangle$

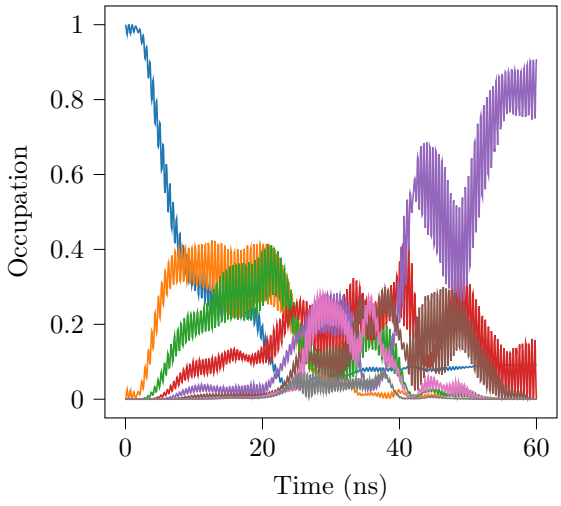

(c) Transfer of $(|0\rangle + |1\rangle)/\sqrt{2}$

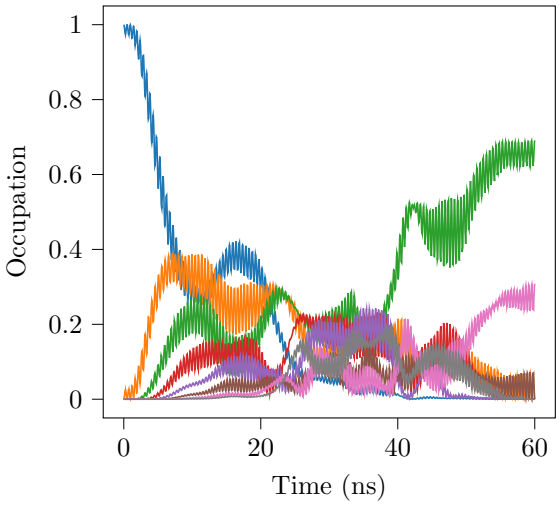

(d) Transfer of $(|0\rangle - |1\rangle)/\sqrt{2}$

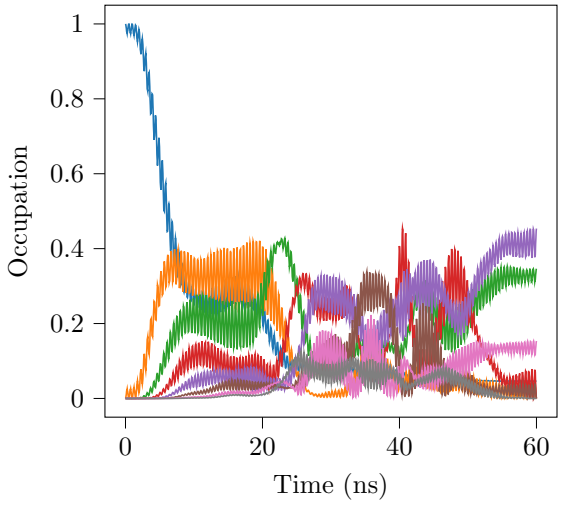

(e) Transfer of $(|0\rangle + i\,|1\rangle)/\sqrt{2}$

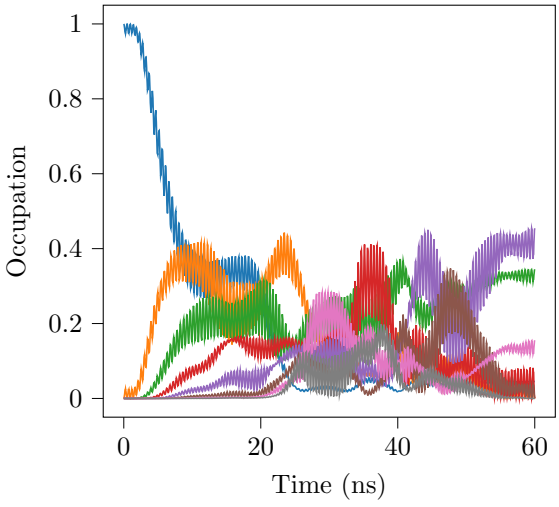

(f) Transfer of $(|0\rangle - i\,|1\rangle)/\sqrt{2}$

Figure A.1: Resonator level occupation over time for the 6 state transfers.